

DOI: 10.1002/adhm.201200078

Article type: Full Paper

Universal Scaling Law to Predict the Efficiency of Magnetic Nanoparticles as MRI T2-Contrast Agents

By

Quoc L. Vuong, Jean-François Berret, Jérôme Fresnais, Yves Gossuin and Olivier Sandre**

Dr. Q. L. Vuong, Author-One,
Université de Mons, Biological Physics Department, 20 Place du Parc, 7000 Mons, Belgium

Dr. J.-F. Berret, Author-Two,
Université Denis Diderot Paris-VII, CNRS UMR7057, Matière et Systèmes Complexes
10 rue Alice Domon et Léonie Duquet, 75013 Paris, France

Dr. J. Fresnais, Author-Three,
UPMC Univ Paris 06, CNRS UMR7195, Physicochimie, Colloïdes et Sciences Analytiques
4 place Jussieu, 75005 Paris, France

[*] Dr. Y. Gossuin, Corresponding-Author,
Université de Mons, Biological Physics Department, 20 Place du Parc, 7000 Mons, Belgium
E-mail: yves.gossuin@umons.ac.be

[*] Dr. O. Sandre, Corresponding-Author,
Université de Bordeaux, CNRS UMR5629, Laboratoire de Chimie des Polymères Organiques
ENSCBP, 16 Avenue Pey Berland, 33607 Pessac, France
E-mail: olivier.sandre@ipb.fr

Keywords: Magnetic Resonance Imaging Contrast Agents; Transverse Relaxivity; Motional Averaging Regime; Static Dephasing Regime; Superparamagnetic Iron Oxide Nanoparticles

Abstract: Magnetic particles are very efficient Magnetic Resonance Imaging (MRI) contrast agents. In the recent years, chemists have unleashed their imagination to design multi-functional nanoprobes for biomedical applications including MRI contrast enhancement. This study is focused on the direct relationship between the size and magnetization of the particles and their nuclear magnetic resonance relaxation properties, which condition their efficiency. Experimental relaxation results with maghemite particles exhibiting a wide range of sizes and magnetizations are compared to previously published data and to well-established relaxation theories with a good agreement. This allows deriving the experimental master curve of the transverse relaxivity *versus* particle size and to predict the MRI contrast efficiency of any type of magnetic nanoparticles. This prediction only requires the knowledge of the size of the particles impermeable to water protons and the saturation magnetization of the corresponding volume. To predict the T_2 relaxation efficiency of magnetic single crystals, the crystal size and magnetization – obtained through a single Langevin fit of a magnetization curve – is the only information needed. For contrast agents made of several magnetic cores assembled into various geometries (dilute fractal aggregates, dense spherical clusters, core-shell micelles, hollow vesicles...), one needs to know a third parameter, namely the intra-aggregate volume fraction occupied by the magnetic materials relatively to the whole (hydrodynamic) sphere. Finally a calculation of the maximum achievable relaxation effect – and the size needed to reach this maximum – is performed for different cases: maghemite single crystals and dense

clusters, core-shell particles (oxide layer around a metallic core) and zinc-manganese ferrite crystals.

1. Introduction

Magnetic Resonance Imaging contrast agents (MRI CAs) allow a high sensitivity for the early detection of different pathologies and the tracking of magnetically tagged cells *in vivo* through molecular and cellular imaging.^[1] The efficiency for MRI CAs consists in lowering the longitudinal (T_1) or transverse (T_2) relaxation times of the nuclear spins of water protons in tissues at the lowest CA concentration, expressed in equivalent mM of magnetic ions. This acceleration of proton magnetization relaxations near a magnetic particle is usually ascribed to fluctuations of magnetic dipolar interactions between the nuclear and the electronic spins. Therefore the “relaxivity” defined as the slope of the relaxation rate in s^{-1} (either T_1 or T_2) versus the equivalent ion concentration in mM is a direct measurement of this efficiency. In the various magnetic nanoparticles or magnetic hybrids proposed so far, authors have interpreted their relaxivity results compared to literature and specifications of commercial products by referring to different notions such as the nature and the size of the Ultra-small Superparamagnetic Iron Oxide (USPIO) grains, the clustering effect (several USPIOs per contrast agent), the influences of a non magnetic shell, of a hydrophobic membrane, of water permeability... In this work, we propose a general treatment of new results and of literature data with a unified method using only two (for individual USPIOs) or three (for clusters or hybrids) parameters: diameter and magnetization of the whole particle, and volume fraction of magnetic materials inside.

2. Magnetic nanoparticles and clusters of various sizes and geometries

2.1. Samples prepared for this study

Magnetic particles and clusters were prepared from USPIO nanoparticles made of maghemite ($\gamma\text{-Fe}_2\text{O}_3$) synthesized in water according to Massart’s procedure (see Experimental).^[2] These nanoparticles were readily dispersed in water and formed a true “ionic ferrofluid”. The iron oxide surface bears positive charges due to adsorption of protons in acidic media, in that case a dilute HNO_3 solution at pH between 1.2 and 1.7. Such ionic ferrofluids remain in a monophasic state under the application of a magnetic field of arbitrary value. On the microscopic scale, those crystals exhibit a Log-Normal distribution of diameters with parameters $d_0 = 7$ nm and $\sigma = 0.38$, as measured by vibrating sample magnetometry (VSM).^[3] Maghemite nanoparticles with such a broad dispersity were treated with a size-sorting procedure based on fractionated phase-separation.^[4] After the increase of ionic strength to induce demixtion and magnetic sedimentation on a strong ferrite magnet, a concentrate could be separated from the supernatant in few minutes. By repeating the phase-separation protocol on both the concentrate and the supernatant, we obtained four new fractions at second level of refined distribution of sizes, and so on after a third and fourth level. To take into account the residual polydispersity, we estimated a weight-averaged diameter characteristic of each sample by calculating the 4th and 3rd order moments of the Log-normal distributions deduced by VSM: $d_w = \langle d^4 \rangle / \langle d^3 \rangle = d_0 \exp(3.5\sigma^2)$. This choice of the characteristic size enabled comparing samples of varying size distributions (even for a same median size d_0). It also fairly compares to the mean diameter observed on the electron microscopy pictures and to twice the gyration radius that can be obtained by a common experiment (Guinier’s plot) from several scattering techniques (light, X-rays or neutrons). After the size-sorting process, the fractions of interest were coated either by coordination bonding of surface iron ions with trisodium citrate (Na_3Cit) ligand^[5] or by electrostatic complexation with sodium polyacrylate (PAA_{2k} or PAA_{5k}) using a precipitation-redispersion protocol.^[6] Superparamagnetic Iron

Oxide (SPIO) particles consisting in spherical clusters of a limited number of individual crystals were also prepared by a coacervation protocol with oppositely charged hydrophilic copolymers controlled by salinity.^[7] Experimental details for the size sorting and coating procedures of the USPIOs and their controlled clustering into SPIO coacervates are described in section 4.

2.2. Samples from literature

Among the huge literature published in the recent years on novel particles as potential MRI contrast agents, we focused our attention on articles reporting precisely the physical (structural, geometrical, magnetic...) properties of the systems. Thus we gathered a broad range of data for individually dispersed maghemite nanoparticles with only a thin permeable coating,^[8–10] maghemite core-silica shell particles,^[11,12] maghemite or magnetite nanoparticles clustered by hydrophilic^[13–15] or amphiphilic^[16–18] polymers, encapsulated in the aqueous lumen of liposomes^[19] or embedded in the membrane of lipid^[20] or polymer^[21] vesicles. Other magnetic materials such as pristine iron–iron/manganese–ferrite core-shell nanoparticles^[22] and manganese–ferrite nanoparticles clusters^[23] were also used to complete our relaxation analysis.

Except for Ultra Ultra-small Superparamagnetic Iron Oxide (UUSPIO) of diameter 4 nm only which can be used as positive contrast agents with T_1 -weighted sequences,^[24] magnetic particles are only effective as T_2 negative contrast agents since at the magnetic fields of most clinical and research MR imagers (1.5 T or above), their longitudinal relaxation rate R_1 falls down due to the absence of the so-called “secular term” in the theoretical expression of R_1 .^[25] Since R_2/R_1 becomes very high, any hyper-signal is lost because of spin-spin relaxation in the transverse plane where the detection antennas are sensitive. This was checked for our samples – by recording the evolution of R_1 on a large range of magnetic fields – confirming the small effect of the particles on water longitudinal relaxation (**Figure S5** in Supporting Information). On the opposite, water transverse relaxation rate R_2 was strongly enhanced by the presence of the samples with no significant variation *versus* magnetic field values between 0.47 and 1.41 T (**Figure S6**).

2.3. Classical relaxation models revisited

For magnetic particles of diameter d and saturation magnetization M_v (corresponding to the total magnetic moment divided by the particle volume and expressed in the SI unit, $A \cdot m^{-1}$), the value of R_2 is given either by the motional averaging regime (MAR) – also called outer sphere theory (as opposite to inner sphere) – or by the static dephasing regime (SDR). But to compare the relaxation data with these models, one needs first to properly define the structure and geometry of the T_2 contrast agent, as depicted by the different cases on **Scheme 1**. We recall here only the final equations of MAR and SDR models, but readers can refer to recent reviews to learn about the quantum mechanics treatment of magnetic dipolar interactions between nuclear and electronic spins which are founding them.^[25]

2.3.1. *Particles in the motional average regime (MAR): $\Delta\omega\tau_D < 1$*

In this case, the protons of freely diffusing water molecules surrounding the particle explore all the possible values of magnetic dipolar field created by the electronic magnetic moment and the transverse relaxation rate at high field is given by:

$$R_2 = \frac{1}{T_2} = \frac{16}{45} f \tau_D (\Delta\omega)^2 \quad (1)$$

where f is the volume fraction occupied by the particles in the suspension, $\Delta\omega = \gamma\mu_0 M_v/3$ is the angular frequency shift experienced by a proton at the equator of the particle, $\gamma = 2.67513 \times 10^8 \text{ rad} \cdot \text{s}^{-1} \cdot \text{T}^{-1}$ the gyromagnetic factor of the proton, $\mu_0 = 4\pi 10^{-7} \text{ T} \cdot \text{m} \cdot \text{A}^{-1}$ the

magnetic permeability of vacuum and $\tau_D = d^2/4D$ the translational diffusion time of the protons in the magnetic field inhomogeneities created by the particles (D being the water translational diffusion constant and d the particle diameter).^[25] To obtain the transverse relaxivity r_2 – defined as the relaxation rate R_2 normalized by the equivalent iron concentration $[\text{Fe}]$ in mM – the volume fraction f should be expressed in terms of equivalent iron concentration. This concept of relaxivity is widely used in the literature to normalize the relaxation rates and compare the efficiencies of different contrast agents. The iron concentration is indeed more direct to measure (by UV-Vis absorption, atomic emission or inductively coupled plasma mass spectroscopy) than the volume fraction occupied by the particles in water. However, normalization by the volume fraction is more rigorous from a theoretical point of view as seen on **Equation (1)**. The numerical factor between f and $[\text{Fe}]$ depends on the type of magnetic material, through its molar volume v_{mat} given by the ratio of the molar mass divided by the number of magnetic ions in the formula and by the mass density, both expressed in SI units to obtain the iron concentration in $\text{mol}\cdot\text{m}^{-3}$ equivalent to $\text{mmol}\cdot\text{L}^{-1}$.

For maghemite ($M_{\gamma\text{-Fe}_2\text{O}_3}=0.1597 \text{ kg}\cdot\text{mol}^{-1}$ and $\rho_{\gamma\text{-Fe}_2\text{O}_3}=5100 \text{ kg}\cdot\text{m}^{-3}$), this writes:

$$f/[\text{Fe}] = v_{\text{mat}} = \frac{M_{\gamma\text{-Fe}_2\text{O}_3}}{2\rho_{\gamma\text{-Fe}_2\text{O}_3}} = 1.57 \times 10^{-5} \text{ m}^3 \cdot \text{mol}^{-1} \quad (2a)$$

and in the general case of an iron spinel $\text{MO}\cdot\text{Fe}_2\text{O}_3$:

$$f/\{[\text{Fe}]+[\text{M}]\} = v_{\text{mat}} = \frac{M_{\text{MO}\cdot\text{Fe}_2\text{O}_3}}{3\rho_{\text{MO}\cdot\text{Fe}_2\text{O}_3}} \approx 1.5 \times 10^{-5} \text{ m}^3 \cdot \text{mol}^{-1} \quad (2b)$$

The nature of the divalent cation in the iron spinel structure (Fe^{2+} , Co^{2+} , Ni^{2+} , Mn^{2+} , Zn^{2+} , ...) varies this result only by $\pm 5\%$. Then equation (1) writes:

$$r_2 = \frac{R_2}{[\text{Fe}]} = \frac{4\gamma^2 \mu_0^2 v_{\text{mat}} M_v^2 d^2}{405 D} \quad (3)$$

which is valid only if the Redfield condition is fulfilled:

$$\Delta\omega\tau_D < 1 \quad (4)$$

This is the case for small single nanoparticles of pure magnetic materials or with a thin fully hydrated shell,^[8-10,13] and for hybrid entities with an overall magnetization (M_v) remaining small compared to the specific magnetization of the inorganic part (m_s), for example dilute micelles^[17] or vesicles^[19,20] containing few iron oxide nanoparticles, or magnetic cores either single^[11] or clustered^[12] wrapped by a rather thick silica coating. In the latter case (porous SiO_2), the permeability of the non magnetic mantle to water molecules can lead to an additional fast mode, but its contribution to the overall relaxation process remains small as long as the water protons diffusing in the “outer shell” represent a larger volume fraction than the internal protons linked to the porous network. For magnetic particles respecting **Equation (4)**, the transverse relaxivity can be divided by M_v^2 to point out the dependence on diameter. Replacing the different constants by their numerical values and using $D = 3 \times 10^{-9} \text{ m}^2\cdot\text{s}^{-1}$ as the water diffusion constant at 37 °C leads to:

$$\frac{r_2}{M_v^2} = a_{\text{theo}} d^2 = 5.9 \times 10^{-12} d^2 \quad (5)$$

To test this relationship, the ratio r_2/M_v^2 was calculated for 9 sizes of single maghemite USPIOs. The values of saturation magnetization M_v ($\text{A}\cdot\text{m}^{-1}$) of all these samples were obtained from the fits of the magnetometry curves with a precise knowledge of the solid volume fraction f in the suspension from an independent titration of iron (also necessary to deduce the relaxivities r_2 in $\text{s}^{-1}\cdot\text{mM}^{-1}$). Data from literature corresponding to various types of ferrite nanoparticles and clusters in the MAR are also presented on Figure 1. For relaxivities

measured at a temperature different from 37 °C, a correction factor corresponding to the tabulated variation of viscosity was applied, reflecting the change of diffusion constant of water molecules.

The values of diameter of the individually dispersed USPIO nanoparticles plotted on the curve are the weight average diameter (d_w) obtained by magnetometry (14 samples) or by TEM (4 samples) or from the simulated curve fitting a T_1 NMRD profile (3 samples). Concerning the clusters, micelles, vesicles and single magnetic cores surrounded by an impermeable non magnetic coating (e.g. silica or polymer), the plotted diameter was either measured by electron microscopy (d_{TEM}) or by dynamic light scattering (d_H) depending on availability in the corresponding references.

For clusters and hybrids, we introduce the intra-aggregate volume fraction of magnetic materials ϕ_{intra} to derive a corrected relaxivity $r_2' = r_2 \times \phi_{intra}$. This normalization for SPIO clusters enables to properly compare their relaxation data $r_2 \times \phi_{intra} / M_v^2$ as if they were filling the same volume fraction of suspension as single USPIO nanoparticles at 1 mM iron concentration. Even though the relaxation efficiency is usually expressed in terms of relaxivity per equivalent mM of iron atoms, the normalization by M_v^2 is theoretically justified for the same total volume fraction of particles f in the suspension, including both parts (iron oxide and impermeable coating). For example with clusters containing $\phi_{intra} = 10\%$ in volume of magnetic nanoparticles, the volume fraction f of clusters in a 1 mM [Fe] suspension will be 10 times larger than for a 1 mM suspension of the dispersed USPIOs. The measured relaxivities should thus be divided by ten to compare the relaxation efficiencies at the same volume fraction of magnetic particles.

Figure 1 shows $r_2 \times \phi_{intra} / M_v^2$ versus d for samples following the MAR model (see **Table 1**), from this study and from literature. This figure presents the normalized relaxivity, obtained as described above, while **Figure S7** (supporting information) directly presents the relaxivity in order to ease the comparison with measured values. Both figures show that samples respecting Equation (4) are indeed quantitatively following a quadratic dependence on diameter over almost two decades (4–300 nm):

$$\frac{r_2 \times \phi_{intra}}{M_v^2} = a_{exp} d^2 = 11.6 \times 10^{-12} d^2 \quad (6)$$

where a_{exp} was obtained by a one-parameter quadratic fit of correlation factor $R=0.93$. The agreement between a_{exp} and a_{theo} values is fairly good, since the size distribution of the nanoparticles – although contained in the weight (d_w) or intensity (d_H) averaged diameter – is expected to influence relaxation and thus the actual value of prefactor a .^[26] Moreover, the diffusion coefficient of bulk water was used to calculate prefactor a_{theo} while water diffusion might be hampered in the vicinity of the particles, as shown in the case of especially hydrophilic polymer shells.^[27] By using the scaling law expressed in **Equation (6)**, it is now possible to predict the transverse relaxivity at magnetic fields above 1 T and at 37 °C of any sample of particles or clusters inducing relaxation in the MAR whose diameter (d_w , d_{TEM} or d_H), magnetic content ϕ_{intra} and saturation magnetization M_v are known, prior to any NMR or MRI measurement. **Figure 1** also presents the data for two samples whose $\Delta\omega\tau_D$ values are slightly larger than 1 and thus appear below the master curve of MAR, as expected.^[10,22] Among these cases, iron-iron oxide core-shell particles^[22] locate slightly below the corresponding particles in the MAR with a similar size $d \approx 15$ nm (see **Table 1**). This is logical since for this sample $\Delta\omega\tau_D = 1.5$, a value corresponding to the transition between MAR and SDR relaxation regimes. Even though r_2/M_v^2 is smaller than predicted, the experimental value $r_2=324 \text{ s}^{-1} \text{ mM}^{-1}$ is twice as large as for a pure iron oxide USPIO of same outer diameter. However, the comparison is somehow complicated by the different stoichiometry and density of both compounds (pristine iron in the core and iron oxide in the

shell), implying different volume fractions f for iron oxide and core-shell particles with identical iron concentration: respectively $f=1.57 \times 10^{-5}$ for iron oxide and $f=10^{-5}$ for $\text{Fe}@\text{Fe}_2\text{O}_3$ at 1 mM equivalent $[\text{Fe}]$, so that the increase of specific magnetization ($M_v=6.6 \times 10^5 \text{ A}\cdot\text{m}^{-1}$ or $115 \text{ emu}\cdot\text{g}^{-1}$) is somehow counterbalanced by the decrease of molar volume v_{mat} .

2.3.2. *Particles out of the motional averaging regime: $\Delta\omega\tau_D > 1$*

For particles with size d and magnetization M_v such that $\Delta\omega\tau_D > 1$, the Static Dephasing Regime (SDR) – implying that water protons explore only a small space compared to the hydrodynamic volume also called “outer shell” around the particle – should be used instead of MAR, yielding a relaxation rate of the form:

$$R_2^* = \frac{1}{T_2^*} = \frac{2\pi}{3\sqrt{3}} f \Delta\omega \approx R_2 \quad (7)$$

With the same transformation as above, one obtains:

$$r_2^* = \frac{R_2^*}{[\text{Fe}]} = \frac{2\pi \gamma \mu_0 v_{\text{mat}} M_v}{9\sqrt{3}} \approx r_2 \quad (8)$$

The SDR model does not take into account the effect of the refocusing pulses used in all T_2 measurement sequences. Therefore **Equation (7)** and **Equation (8)** are only exact for R_2^* and r_2^* respectively, which determine the signal contrast in MR imaging conditions without spin echoes (*e.g.* with gradient echoes sequences). Nevertheless, the SDR formulas (7) and (8) give good approximations of R_2 and r_2 as long as $5 < \Delta\omega\tau_D < 20$ and provide good estimate of the maximum values reached in the middle of the SDR range, when $\Delta\omega\tau_D \approx 10$.^[26] Above an upper limit $\Delta\omega\tau_D \approx 20$, R_2 is no more approximated by the SDR, since the refocusing pulses used in the T_2 measurement sequence become effective. In this third relaxation regime described by the Partial Refocusing Model (PRM), R_2 is lower than R_2^* and exhibits a strong dependence on the echo time chosen for the measuring sequence.^[28]

For particles with characteristics corresponding to $1 < \Delta\omega\tau_D < 5$, neither **Equation (3)** nor Equation (8) is valid and a transition between MAR and SDR relaxation is observed. As $\Delta\omega\tau_D > 20$, one observes a transition between SDR and PRM. **Figure 2** represents the normalized relaxivities $r_2' = r_2 \times \phi_{\text{intra}}$ for all the systems with $\Delta\omega\tau_D > 1$ (see Table 1). Only particles of approximately same M_v can be compared together. The figure also gives – for different M_v ranges – the predictions of the empirical function recently validated by computer simulations for particles outside the MAR.^[26] The trend of these empirical curves is compatible with the experimental data. It should be stressed that the comparison between all the samples – and also with theory – is difficult since these systems are in a “theoretical no-man’s-land” and also because, for many samples, R_2 surely depends on the echo-time of the measurement sequence. Nevertheless, most experimental data are located in the domains of Figure 2 corresponding to their size and magnetization, except those derived from the article by C. Paquet *et al* on magnetic hydrogels,^[15] which show higher $r_2 \times \phi_{\text{intra}}$ values than expected from the simulations (for particle sizes $\sim 150 \text{ nm}$ and 175 nm). The simulations shown here do not take into account the mechanism reported recently for highly hydrated particles.^[27] In that case, the slowing down of proton diffusion near the magnetic particle surface – where the magnetic gradients are the strongest – induces fast proton dephasing, which significantly raises the relaxivity.^[27] The present study holds for the two limit cases of either impermeable coatings or completely permeable shells. Therefore “smart” coatings modifying proton diffusion such as the magnetic hydrogels somehow deviate from the general behavior.

2.3.3. *Maximal achievable transverse relaxivities*

As learned from computer simulations^[26] and supported by the data presented in Figure 2, the relaxation enhancement effect of magnetic particles is expected to reach a maximum value for

a particular size. This maximum occurs when the system is completely in the SDR. As previously stated, this is the case when $\Delta\omega\tau_D \approx 10$. It is thus possible to estimate, using Equation (8), the maximum efficiency of different types of magnetic particles as well as the optimal size at which this maximum should be reached. The results, obtained by using the expressions of $\Delta\omega$ and τ_D , are presented in **Table 2**.

The first important information obtained from Table 2 is that the maximum relaxivity is the same for maghemite nanoparticles and clusters of maghemite particles, only the optimal size of particles needed to reach the maximum is different (obtained through the condition $\Delta\omega\tau_D \approx 10$). In the case of individual magnetic cores, such a diameter of 55 nm falls above the classical limit size of 40 nm for USPIOs defined relatively to the sizes of biological barriers, but remains below the maximum size of magnetic (Weiss) monodomains.^[25] Moreover, it will be a challenge to reach it experimentally in a proper dispersed (colloidal) state because of strong inter-particle attractions. In the literature, different clusters of γ -Fe₂O₃ or Fe₃O₄ cores^[15-18] plotted on Figure 2 already exceeded a T_2 relaxivity of 500 s⁻¹·mM⁻¹ but remained below the theoretical maximum of 750 s⁻¹·mM⁻¹ not yet reached experimentally, according to the authors' knowledge. Other studies presenting dense magnetite clusters around 100 nm only show a moderate increase of r_2 compared to the individual USPIOs,^[29] presumably due to too high size dispersity. Secondly and as expected,^[22,30] core-shell or special compositions of ferrite particles with a higher saturation magnetization than pure iron oxide led to higher relaxivities. It was recently proven that an appropriate composition of zinc and manganese ferrite enables reaching $r_2=860$ s⁻¹·mM⁻¹ for a diameter $d=15$ nm.^[30] According to Table 2, r_2 should reach even larger values (up to 1200–1860 s⁻¹·mM⁻¹) by increasing the size both for Fe@Fe₂O₃ core-shells and (Zn_{0.4}Mn_{0.6})Fe₂O₄ mixed ferrite nanoparticles. Increasing the specific magnetization of USPIOs by an appropriate choice of their metal composition is indeed an interesting option to optimize MRI contrast agents, as long as toxicity is not introduced by the non ferrous metals.

3. Conclusions

Despite the broad variety of superparamagnetic MRI contrast agents differing by their size, geometry (filled micelles or hollow vesicles, dense or loose clusters...), type of coating (organic or inorganic, impermeable or porous, hydrophilic or hydrophobic...), no specific models need to be introduced. We have indeed evidenced in this article that the classical MAR and SDR models can correctly represent the experimental data once structural and magnetic parameters are known (external diameter, volume fraction and magnetization of the magnetic materials) and the relaxivity is appropriately normalized. More precisely, the MAR is verified by individual USPIOs or clusters which are either compact or diluted in a non magnetic material. In the latter case, the porosity (*e.g.* silica) or permeability to water (*e.g.* hydrogel) is not an issue: such internal protons relax much faster than external ones, but their contribution to the measured relaxation rate remains limited due to their low volume fraction compared to the water protons diffusing in the “outer shell” around the particle. The relaxivity at high magnetic field / Larmor frequency of particles in the MAR follows a universal scaling law varying with the square of diameter, square of magnetization and inverse of the internal volume fraction of magnetic material. The experimental prefactor of this power law is in good accordance with the physical constants of the models. For larger or more concentrated clusters, the SDR model correctly describes the plateau value that is observed experimentally. Moreover, the size and magnetization of the particle can be chosen to satisfy the condition $\Delta\omega\tau_D \approx 10$ in order to design contrast agents of maximum T_2 relaxivity.^[26] But it should be stressed that this optimum r_2 will only be approached by particles presenting a rather narrow size distribution centered on the optimal size, since smaller (in motional averaging regime) and larger particles (following the Partial Refocusing Model) will present lower efficiencies

and decrease the mean transverse relaxivity of the sample. This explains why some already reported SPIO clusters did not exhibit tremendous r_2 despite mean values of magnetization, volume fraction and hydrodynamic diameter close to the optimal ones.^[29]

To conclude, by validating simple principles of the theory of proton relaxation on a wide range of experimental systems, this article proposes a unified method to predict the transverse relaxivity r_2 of MRI contrast agents at clinical field based on materials (M_v) and geometrical (d, ϕ_{intra}) parameters. These results offer practical tools to the chemists who aim at optimizing the relaxation properties for MRI in the design of more elaborated particles than the commercially available T_2 contrast agents, such as multi-modal probes or theranostic nanovectors.

4. Experimental

Synthesis of Ultra-small Superparamagnetic Iron Oxide. USPIO nanoparticles made of maghemite ($\gamma\text{-Fe}_2\text{O}_3$) were synthesized in water according to Massart's procedure.² At first, magnetite Fe_3O_4 nanocrystals (also called ferrous ferrite $\text{FeO}\cdot\text{Fe}_2\text{O}_3$) were prepared from an alkaline coprecipitation of a quasi-stoichiometric mixture of iron +II (0.9 mol) and iron +III (1.5 mol) chloride salts in HCl solution (3L, $\text{pH}\approx 0.4$). One liter of a concentrated ammonia solution (7 mol) was quickly added onto the acidic iron salts mixture, which produced a black solid suspension almost instantaneously. After 30 minutes of stirring at 800 rpm, the Fe_3O_4 nanoparticles were attracted by a strong ferrite magnet ($152\times 101\times 25.4\text{ mm}^3$, Calamit Magneti, Milano-Barcelona-Paris). Then the supernatant ($\approx 2.25\text{ L}$) containing non magnetic ferrihydrites (reddish flakes) was discarded and the magnetic precipitate (black) was washed with 1 L water. After sedimentation on the ferrite magnet, the flocculate was acidified with 0.26 L of nitric acid (69%) and stirred 30 min after being completed up to 2 L with water. In order to be completely oxidized from magnetite into maghemite, the solid phase was separated from the supernatant ($\approx 1.5\text{ L}$, red) and immersed in a boiling solution of ferric nitrate (0.8 mol in 0.8 L). After 30 min under stirring at 90-100 °C, the suspension had turned into the red colour characteristic of maghemite $\gamma\text{-Fe}_2\text{O}_3$. After washing steps in acetone and diethyl-ether to remove the excess ions, the nanoparticles readily dispersed in water and formed a true "ionic ferrofluid" made of maghemite nanoparticles. The iron oxide surface bore positive charges due to adsorption of protons in acidic media, in that case a dilute HNO_3 solution at pH between 1.2 and 1.7. Therefore such ferrofluid remains in a monophasic state under the application of a magnetic field of arbitrary value.^[2-5]

Size sorting. On the microscopic scale, those crystals exhibit a Log-Normal distribution of diameters of parameters $d_0=7\text{ nm}$ and $\sigma=0.38$, as measured by magnetometry.^[3] Maghemite nanoparticles with such a high size-dispersity can be treated with a size-sorting procedure based on fractionated phase-separation.^[4] More precisely, the addition of an excess of HNO_3 not only lowers the pH but also raises the ionic strength, thereby screening the electrostatic repulsions between the nanoparticles. Above a threshold electrolyte concentration, a liquid-liquid phase separation occurs between a concentrated "liquid-like" phase and a dilute "gas-like" phase. After magnetic sedimentation on a strong ferrite magnet ($152\times 101\times 25.4\text{ mm}^3$, Calamit Magneti, Milano-Barcelona-Paris) to accelerate demixtion, a concentrate (denoted C1) could be readily separated from the supernatant (denoted S1). Once washed with acetone to remove the excess of ions, the two separated fractions were dispersed in water. The fit of their magnetization curve by VSM leads to their size distributions modelled by a Log-normal law with d_0 as median diameter and σ as standard width of the logarithms of diameters: $d_0 = 8.7\text{ nm}$ ($\sigma=0.35$) for C1 and $d_0 = 7.1\text{ nm}$ ($\sigma=0.29$) for S1. The enrichment of the "liquid-like" phase by the larger size tail of the distribution compared to the dilute "gas-like" phase originates from the sensitivity of the inter-nanoparticle potential with the diameters (the larger nanoparticles exhibiting much higher Van der Waals interactions between them). By

repeating the phase-separation protocol on both samples C1 and S1, we obtained four new fractions at second level of refined distribution of sizes, and so on after a third and fourth level as indicated on **Sketch S1**, among which several fractions were used in the following of the article either as they were in nitric acid conditions (C1S2, C1C2C3, C1C2S3, S1S2C3) or after coating with citrate or polyacrylate ligands (S1S2S3, S1S2C3, C1C2C3C4). Unlike the preceding steps for which fractions were divided into culots (C) and supernatants (S) by phase separation under increased HNO₃ concentration, for the final step C1C2C3C4S5 another method was used. Namely S5 stands in that case for “sedimentation”: a strong magnetic gradient was used indeed to induce a vertical concentration gradient (but not a true separation into 2 phases as with the electrolyte). A colloidal suspension enriched in the largest magnetic nanoparticles was pipetted at the bottom of the cuvette.^[31] After the size-sorting process, the fractions of interest (S1S2S3, S1S2C3, C1C2C3C4 and C1C2C3S4) were coated either with tri-sodium citrate^[5] Na₃Cit or sodium polyacrylate^[6,32] (PAA_{2k} or PAA_{5k}) using a protocol based on electrostatic complexation and adsorption.

Coating with citric acid. Briefly, the grafting was made by reacting 37.4 g of Na₃Cit per mole of iron oxide (20% molar) around pH 8 for 30 min at 70 °C under vigorous stirring and subsequent removal of the supernatant by magnetic sedimentation. Then three washing cycles were performed with acetone to remove the excess ions and finally with diethyl ether to remove acetone. The obtained precipitate of citrate-coated USPIOs can be readily suspended in pure water by simple vortexing. To insure a perfect colloidal stability with low hydrodynamic diameters as probed by dynamic light scattering, the salinity caused by unbound citrate ions was decreased by dialysis for 24 hours against 8 mM Na₃Cit.

Coating with Poly(acrylic acid). Poly(sodium acrylate), the salt form of polyacrylic acid, with a molar mass $M_n = 2000 \text{ g mol}^{-1}$ (PAA_{2k}) or $M_n = 5000 \text{ g mol}^{-1}$ (PAA_{5k}) and a polydispersity index $M_w/M_n = 1.7$ was purchased from Sigma Aldrich (references 81130 and 81132) and used without further purification. In order to adsorb polyelectrolytes onto the surface of the nanoparticles, we followed the “precipitation-redispersion” protocol.^[6,32] The precipitation of the cationic iron oxide dispersion by PAA_{2k/5k} was performed in acidic conditions (pH 2) at weight concentrations of 1 g·L⁻¹ for both nanoparticles and polymer. The precipitate was separated from the solution by centrifugation, and its pH was increased by addition of ammonium hydroxide. The precipitate redispersed spontaneously at pH ≈ 7–8, yielding a clear solution that now contained the polymer-coated particles. The hydrodynamic sizes of γ -Fe₂O₃ USPIOs coated by PAA_{2k} were found to be 5 nm larger than the hydrodynamic diameter of the uncoated particles, indicating a corona thickness $h = 2.5 \text{ nm}$.^[32] In terms of coverage, the number of adsorbed chains per particle was estimated to be 1 nm⁻² (assuming a 1:1 PAA_{2k}-iron oxide weight ratio for an USPIO of molar mass ≈ 10⁶ g·mol⁻¹ and surface ≈ 500 nm²). As a final step, the dispersions were dialyzed against DI-water which pH was first adjusted to 8 (Spectra/Por 2 dialysis membrane with MWCO 12 kD). At this pH, 90 % of the carboxylate groups of the PAA coating were ionized. Electrophoretic mobilities were found at values $\mu_E = -3.76 \times 10^{-4}$ and $-3.52 \times 10^{-4} \text{ cm}^2 \text{ V}^{-1}$ for Cit- γ -Fe₂O₃ and PAA_{2k}- γ -Fe₂O₃ respectively. As a final step of the procedures described above, the dispersions were dialyzed against DI-water which pH was first adjusted to 8 by addition of sodium hydroxide (Spectra Por 2 dialysis membrane with MWCO 12 kD). For the citrate-coated particles, DI-water was supplemented with 8 mM of free citrates. At this pH, 90 % of the carboxylate groups of the citrate and PAA_{2K} coating were ionized. The suspension pH was adjusted with reagent-grade nitric acid (HNO₃) and with sodium or ammonium hydroxides. For the assessment of the stability with respect to ionic strength (I_s), sodium and ammonium chloride (NaCl and NH₄Cl, Fluka) were used to control I_s in the range 0 – 1 M.^[32]

Clustering. Different clusters were prepared with the S1S2C3 iron oxide cores. The principle consists in mixing negatively charged USPIOs coated with PAA and a double-hydrophilic

diblock copolymer (DHBC) such as poly(trimethylammonium ethylacrylate methylsulfate)-*b*-polyacrylamide (PAM_{30k}-*b*-PTEA_{11k}) made of a neutral block (PAM) and a cationic block (PTEA) at a high salt concentration where the electrostatic interactions are totally screened. When the salinity is decreased at a controlled rate either by dilution or dialysis, below a threshold concentration ($[\text{NH}_4\text{Cl}] = 0.4 \text{ mol/L}$) a microphase separation occurs by association between the oppositely charged species. The coacervates are perfectly spherical, with a magnetic core containing a limited number of USPIOs wrapped by a neutral polymer shell that prevents further aggregation. Different clusters of varying size and magnetization can be prepared by varying the salinity decrease rate.^[32] For example, spherical SPIO particles containing approximately 70 iron oxide crystals with a hydrodynamic diameter of 127 nm (see also TEM picture on **Figure S2**) were obtained by mixing S1S2C3@PAA_{2k} USPIOs ($0.75 \text{ g}\cdot\text{L}^{-1}$) and PAM_{30k}-*b*-PTEA_{11k} ($1.5 \text{ g}\cdot\text{L}^{-1}$) in $0.43 \text{ mol}\cdot\text{L}^{-1} \text{ NH}_4\text{Cl}$ and diluting 3 times with pure water (down to $0.143 \text{ mol}\cdot\text{L}^{-1} \text{ NH}_4\text{Cl}$). Iron oxide represents 33 % w/w of these hybrid particles and thus an average volume fraction of 6 % v/v only.

Vibrating sample magnetometry. A laboratory made VSM instrument was used, measuring the magnetization curve *versus* excitation $M(H)$ at RT for a magnetic suspension of volume fraction f from the signal induced in detection coils when the sample is moved periodically in an applied magnetic field varied from 0 to 1 T (thanks to synchronous detection and with an appropriate calibration to convert the signal in mV into $\text{A}\cdot\text{m}^{-1}$).

Dynamic light scattering. DLS measurements were performed on a Malvern NanoZS apparatus operating at a 173° scattering angle. The collective diffusion coefficient D was determined from the second-order autocorrelation function of the scattered light. From the value of the coefficient, the hydrodynamic diameter of the colloids was calculated according to the Stokes-Einstein relation, $d_H = k_B T / 3\pi\eta_s D$, where k_B is the Boltzmann constant, T the temperature ($T = 298 \text{ K}$) and η_s the solvent viscosity ($\eta_s = 0.89 \times 10^{-3} \text{ Pa}\cdot\text{s}$ for water). The autocorrelation functions were interpreted using the 2nd order cumulants (Z -average diameter and Poly-Dispersity Index) and the multimodal fit provided by the instrument software.

Relaxometry. Relaxation time measurements were performed at low fields on BRUKER (Germany) mq 20, mq 60 instruments and a Spintrack relaxometer operating at magnetic fields (B_0) of 0.47, 1.41, 0.67 and 0.93 T respectively. BRUKER AVANCE-200 (4.7 T), BRUKER AMX 300 (7 T) and AMX 500 (11.7 T) spectrometers were used for the high-field T_1 measurements. T_1 relaxation profiles were recorded at 5°C and 37°C from 0.00023 to 0.23 T on a Spinmaster fast field cycling relaxometer (STELAR, Mede, Italy). In most of the graphs, the magnetic field is expressed in term of proton Larmor frequency: a field of 1 Tesla corresponds to a Larmor frequency of 42.6 MHz. The results are expressed as longitudinal and transverse relaxivities which are defined by the increase in the longitudinal and transverse relaxation rates due to an increase of 1 mM in the paramagnetic ion concentration. The relaxivity values were properly calculated by an accurate titration of the iron content in all samples as determined using Inductively Coupled Plasma Atomic Emission spectroscopy (Thermo, USA), after micro-wave mineralization of the suspensions with a mixture of nitric acid and hydrogen peroxide. Varying shapes of the T_1 profiles reflect the differences in sizes, magnetizations and Néel relaxation times of the particles.^[33] T_2 was measured with a CPMG sequence using an inter-echo time of 1 ms. T_2^* was not measured for our samples. Indeed, different tests on the high resolution spectrometers showed that even for reference solutions (simply containing gadolinium ions, for example), the value of T_2^* evaluated with the line-width of the resonance peak was always significantly lower than the T_2 value, while for such systems T_2 and T_2^* should be identical. The influence of the shims seems to be critical when estimating T_2^* with this technique. For strongly magnetic compounds, the measurement of a “real” T_2^* , comparable to the value predicted by the different microscopic relaxation theories, could be very difficult.

Numerical simulation. The empirical expression used to plot the solid curves on Figure 2 was validated by a previously described Monte Carlo simulation of T_2 decay at high fields.^[26] The methodology consists mainly in three steps. Firstly, static and impenetrable spherical magnetic particles are distributed in the simulation space. Secondly, the diffusion of each proton is simulated by a random walk. At each time step, the spin dephasing of each proton – proportional to local dipolar magnetic field produced by the particles – is computed. Finally, the MR signal decay is obtained by averaging all the protons spins and an exponential law can be fitted to the data to obtain the transverse relaxation rate r_2 .

Supporting Information

Supporting Information is available online from the Wiley Online Library or from the author. S1. Synoptic scheme of the size sorting procedure. S2. Characterization of the nanoparticles: a) Magnetometry; b) Transmission Electron Microscopy; c) NMR Relaxometry.

Acknowledgements

Author-One and Author-Four are grateful to Dr Alain Roch for helpful discussions and to Prof. Dr. Robert N Muller for the access to the 60 MHz relaxometer. Authors also thank Aude Michel and Delphine Talbot (PECSA) respectively for TEM and iron atomic emission spectroscopy. This research was supported in part (UMONS) by the Fonds de la Recherche Scientifique (IISN 4.4507.10), (MSC/PECSA/LCPO) by the Agence Nationale de la Recherche under the contracts BLAN07-3_206866 “ITC-nanoProbe”, and (MSC/PECSA) by the European Community through the project “NANO3T—Biofunctionalized Metal and Magnetic Nanoparticles for Targeted Tumor Therapy”, project number 214137 (FP7-NMP-2007-SMALL-1). Author-One is a research fellow from FRS-FNRS.

Annotations

CA, contrast agents; CPMG, Carr-Purcell-Meiboom-Gill; DLS, dynamic light scattering; MAR, motional averaging regime; MRI, magnetic resonance imaging; NMRD, nuclear magnetic resonance dispersion; OS, outer sphere; SDR, static dephasing regime; SI, système international d’unités; SPION, superparamagnetic iron oxide nanoparticle; USPIO, ultra-small superparamagnetic iron oxide; VSM, vibrating sample magnetometry.

Received: ((will be filled in by the editorial staff))

Revised: ((will be filled in by the editorial staff))

Published online: ((will be filled in by the editorial staff))

[1] a) J. A. Frank, H. Zywicke, E. K. Jordan, J. Mitchell, B. K. Lewis, B. Miller, L. H. Jr Bryant, J. W. Bulte, *Acad. Radiol.* **2002**, *9*, S484; b) C. Billotey, C. Wilhelm, M. Devaud, J-C. Bacri, J. Bittoun, F. Gazeau, *Magn. Res. Med.* **2003**, *49*, 646; c) P. Smirnov, F. Gazeau, J-C. Beloeil, B. T. Doan, C. Wilhelm, B. Gillet, *Contrast Med. Mol. Imaging* **2006**, *1*, 165; d) H. B. Na, I. C. Song, T. Hyeon, *Adv. Mater.* **2009**, *21*, 2133; e) F. Xu, C. Cheng, F. Xu, C. Zhang, H. Xu, X. Xie, D. Yin, H. Gu, *Nanotechnology* **2009**, *20*, 405102.

[2] R. Massart, *IEEE Trans. Mag.* **1981**, *17*, 1247.

[3] R. W. Chantrell, J. Popplewell, S. W. Charles, *IEEE Trans. Mag.* **1978**, *14*, 975.

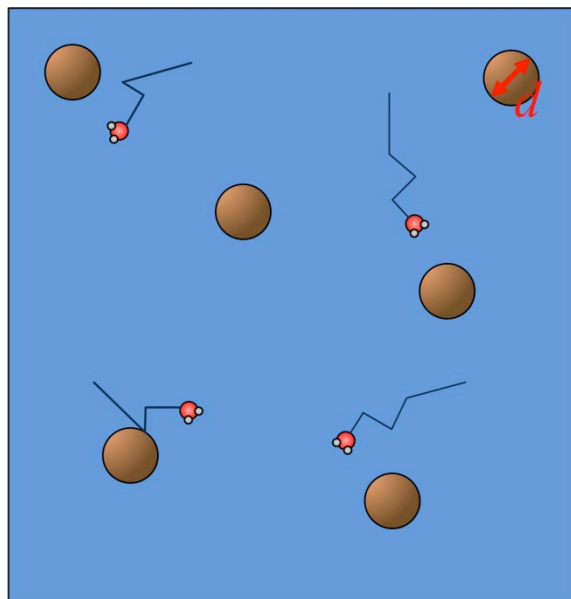
[4] a) J-C. Bacri, R. Perzynski, D. Salin, V. Cabuil, R. Massart, *J. Coll. Int. Sci.* **1989**, *132*, 43; b) R. Massart, E. Dubois, V. Cabuil, E. Hasmonay, *J. Magn. Magn. Mater.* **1995**, *149*, 1.

[5] J. A. Galicia, O. Sandre, F. Cousin, D. Guemghar, C. Ménager, V. Cabuil, *J. Phys. Cond. Mat.* **2003**, *15*, S1319.

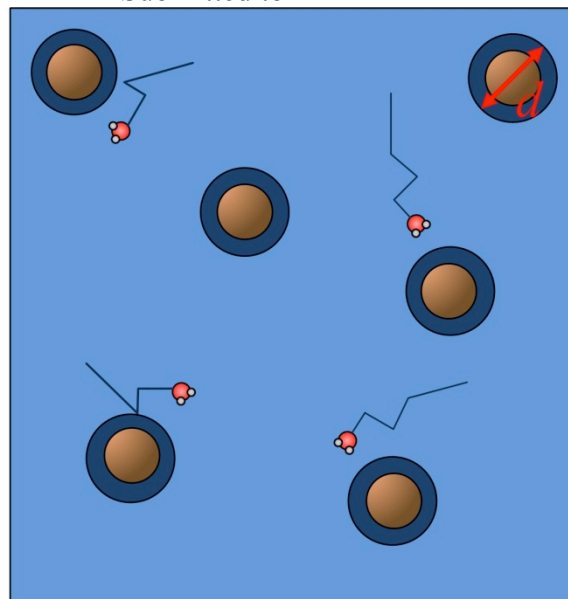
[6] A. Sehgal, Y. Lalatonne, J-F. Berret, M. Morvan, *Langmuir* **2005**, *21*, 9359.

- [7] J. Fresnais, J-F. Berret, B. Frka-Petescic, O. Sandre, R. Perzynski, *Adv. Mater.* **2008**, *20*, 3877.
- [8] D. Forge, Y. Gossuin, A. Roch, S. Laurent, L. Vander Elst, R. N. Muller, *Contrast Med. Mol. Imaging* **2010**, *5*, 126.
- [9] S. H. Koenig, K. E. Kellar, D. K. Fujii, W. H. H. Gunther, K. Briley-Saebø, M. Spiller, *Acad. Radiol.* **2002**, *9*, S5.
- [10] L. Lartigue, C. Innocenti, T. Kalaivani, A. Awwad, M. del Mar Sanchez Duque, Y. Guari, J. Larionova, C. Guérin, J-L. Georges Montero, V. Barragan-Montero, P. Arosio, A. Lascialfari, D. Gatteschi, C. Sangregorio, *J. Am. Chem. Soc.* **2011**, *133*, 10459.
- [11] S. L. Pinho, G. A. Pereira, P. Voisin, J. Kassem, V. Bouchaud, L. Etienne, J. A. Peters, L. Carlos, S. Mornet, C. F. Geraldés, J. Rocha, M.-H. Delville, *ACS Nano* **2010**, *4*, 5339.
- [12] E. Taboada, R. Solanas, E. Rodríguez, R. Weissleder, A. Roig, *Adv. Funct. Mater.* **2009**, *19*, 2319.
- [13] C. W. Jung, P. Jacobs, *Magn. Reson. Imaging.* **1995**, *13*, 661.
- [14] J-F. Berret, N. Schonbeck, F. Gazeau, D. El kharrat, O. Sandre, A. Vacher, M. Airiau, *J. Am. Chem. Soc.* **2006**, *128*, 1755.
- [15] C. Paquet, H. W. de Haan, D. M. Leek, H.-Y. Lin, B. Xiang, G. Tian, A. Kell, B. Simard, *ACS Nano* **2011**, *5*, 3104.
- [16] H. Ai, C. Flask, B. Weinberg, X. Shuai, M. D. Pagel, D.; Farrell, J. Duerk, J. Gao, *Adv. Mater.* **2005**, *17*, 1949.
- [17] Y. Wang, Y. W. Ng, Y. Chen, B. Shuter, J. Yi, J. Ding, S-C. Wang, S-S. Feng, *Adv. Funct. Mater.* **2008**, *18*, 308.
- [18] X. Xie, C. Zhang, *J. Nanomaterials* **2011**, 152524.
- [19] M.-S. Martina, J-P. Fortin, C. Ménager, O. Clément, G. Barratt, C. Grabielle-Madelmont, F. Gazeau, V. Cabuil, S. Lesieur, *J. Am. Chem. Soc.* **2005**, *127*, 10676.
- [20] G. Beaune, M. Levy, S. Neveu, F. Gazeau, C. Wilhelm, C. Ménager, *Soft Matter* **2011**, *7*, 6248.
- [21] C. Sanson, O. Diou, J. Thévenot, E. Ibarboure, A. Soum, A. Brûlet, S. Miraux, E. Thiaudière, S. Tan, A. Brisson, V. Dupuis, O. Sandre, S. Lecommandoux, *ACS Nano* **2011**, *5*, 1122.
- [22] a) S. Cheong, P. Ferguson, K. W. Feindel, I. F. Hermans, P. T. Callaghan, C. Meyer, A. Slocombe, C-H. Su, F-Y. Cheng, C-S. Yeh, B. Ingham, M. F. Toney, R. D. Tilley, *Angew. Chem. Int. Ed.* **2011**, *50*, 4206; b) T-J. Yoon, H. Lee, H.; Shao, R. Weissleder, *Angew. Chem. Int. Ed.* **2011**, *50*, 4663.
- [23] a) J. Yang, C-H. Lee, H-J. Ko, J.-S. Suh, H-G. Yoon, K. Lee, Y-M. Huh, S. Haam, *Angew. Chem. Int. Ed.* **2007**, *46*, 8836; b) E-K. Lim, Y-M. Huh, J. Yang, K. Lee, J-S. Suh, S. Haam, *Adv. Mater.* **2011**, *23*, 2436.
- [24] U. I. Tromsdorf, O. T. Bruns, S. C. Salmen, U. Beisiegel, H. Weller, *Nano Lett.* **2009**, *9*, 4434.
- [25] a) P. Gillis, A. Roch, R. A. Brooks, *J. Magn. Reson.* **1999**, *137*, 402; b) S. Laurent, D. Forge, M. Port, A. Roch, C. Robic, L. Vander Elst, R. N. Muller, *Chem. Rev.* **2008**, *108*, 2064; c) Y. Gossuin, P. Gillis, A. Hocq, Q. L. Vuong, A. Roch, *WIREs Nanomed. Nanobiotechnol.* **2009**, *1*, 299; d) M. R. J. Carroll, R. C. Woodward, M. J. House, W. Y. Teoh, R. Amal, T. L. Hanley, T. G. St Pierre, *Nanotechnology* **2010**, *21*, 035103.
- [26] Q. L. Vuong, P. Gillis, Y. Gossuin, *J. Magn. Reson.* **2011**, *212*, 139.
- [27] H. W. de Haan, C. Paquet, *Magn. Reson. Med.* **2011**, *66*, 1759.
- [28] P. Gillis, F. Moiny, R. A. Brooks, *Magn. Reson. Med.* **2002**, *47*, 257.
- [29] B. A. Larsen, M. A. Haag, N. J. Serkova, K. R. Shroyer, C. R. Stoldt, *Nanotechnology* **2008**, *19*, 265102.

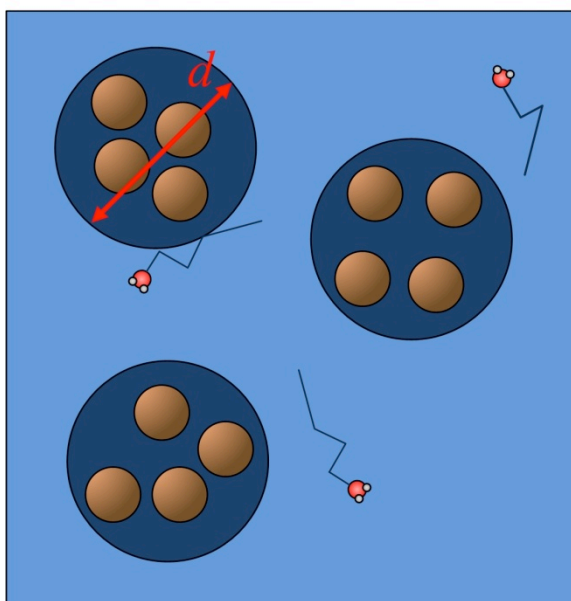
- [30] J. Jang, H. Nah, J-H. Lee, S. H. Moon, M. G. Kim, J. Cheon, *Angew. Chem. Int. Ed.* **2009**, *48*, 1234.
- [31] J-F. Berret, O. Sandre, A. Mauger, *Langmuir* **2007**, *23*, 2993.
- [32] B. Chanteau, J. Fresnais, J-F. Berret, *Langmuir* **2009**, *25*, 9064.
- [33] A. Roch, R. N. Muller, P. Gillis, *J. Chem. Phys.* **1999**, *110*, 5403.



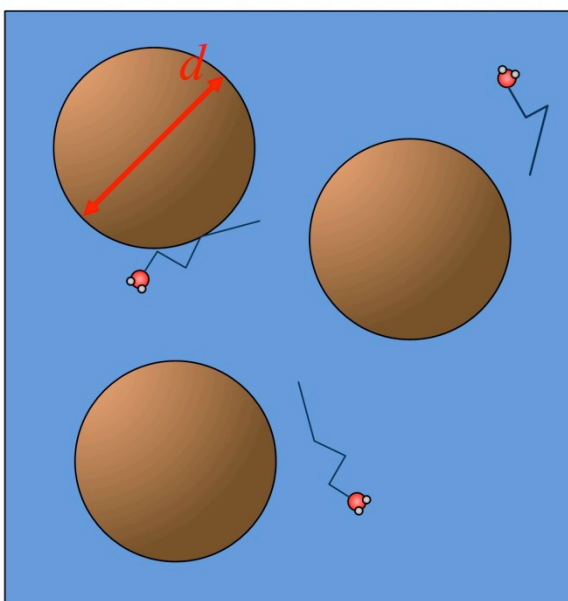
(a)



(b)



(c)



(d)

Scheme 1. In the commonly used relaxation models, d is defined as twice the minimum approach distance of a water molecule to the center of the contrast agent. For a single nanoparticle, d is equal to its diameter (case a). If there is a layer inaccessible to water molecules (case b), d must include this impermeable coating thickness (dark blue shell). If nanoparticles are clustered (case c), d corresponds to the whole hydrodynamic diameter, determined by dynamic light scattering. The MAR model can predict the relaxivities induced by such systems, assimilating the cluster to a single magnetic particle with adapted diameter d and magnetization M_v (case d). But in order to compare with MAR equations, the r_2 relaxivity has to be multiplied by the intra-aggregate volume fraction ϕ_{intra} to get a corrected relaxivity r_2' induced by the aggregate (see text).

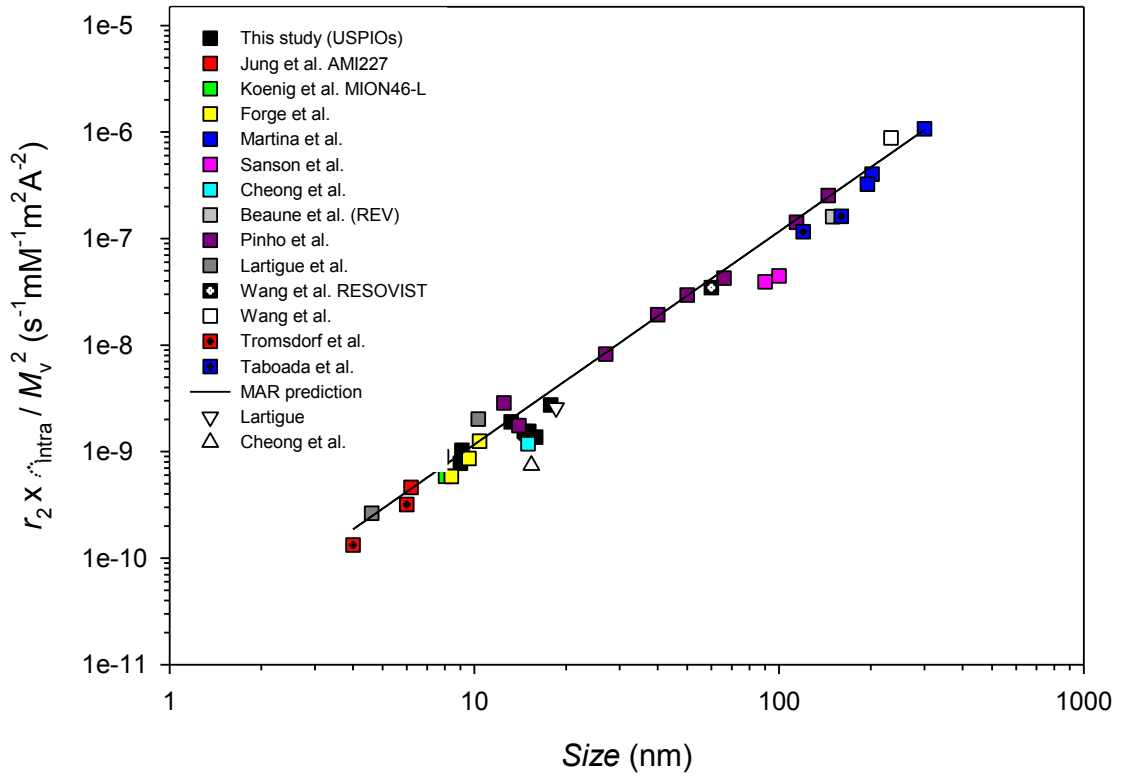


Figure 1. Samples in the motional averaging regime (MAR), with $\Delta\omega\tau_D < 1$. Influence of the size on transverse relaxivity at high field ($\geq 1\text{T}$) and at 37°C with the appropriate weighting by the intra-aggregate volume fraction ϕ_{intra} and normalization by the square of the magnetization enabling to compare USPIOs (single cores), maghemite core-silica shell particles, magnetic vesicles and SPIOs (clusters) on the same curve. The solid line is Equation (6).

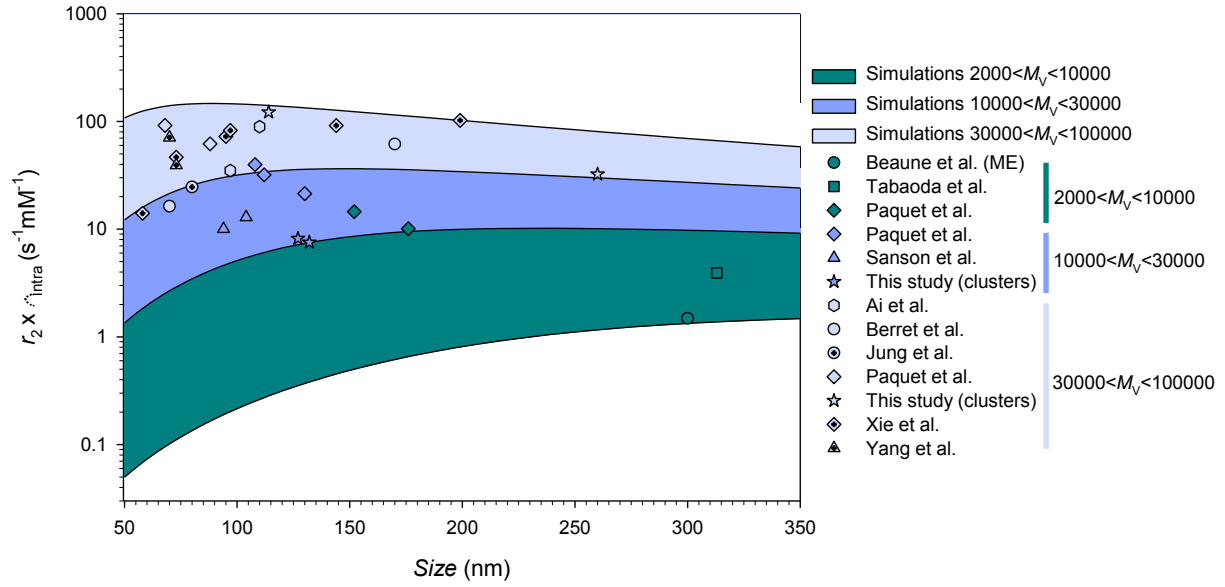


Figure 2. Samples out of the MAR, with $\Delta\omega\tau_D > 1$. Influence of the size on transverse relaxivity at high field ($\geq 1\text{T}$) and at 37°C with the appropriate weighting by the intra-aggregate volume fraction ϕ_{intra} . The colored regions correspond to the relaxivities obtained by computer simulations, through the use of an empirical function which was recently validated.^[26]

Table 1 summarizes the parameters used for the samples presented in **Figure 1** and **Figure 2**.

Reference	Sample code	Magnetic materials	Nature of coating	Size (nm)	Method	ϕ_{intra}	M_v (A.m ⁻¹)	r_2 (s ⁻¹ .mM ⁻¹)	$\phi_{\text{intra}} r_2 M_v^{-2}$ (s ⁻¹ .mM ⁻¹ A ⁻² .m ²)	$\Delta\omega\tau_D$	
In motional averaging regime – $\Delta\omega\tau_D < 1$											
This study	S1S2S-PAA2k	γ -Fe ₂ O ₃	Hydrophilic Polymer (PAA2k or PAA5k)	7.8	VSM-d _w	1	280000	70	8.9.10 ⁻¹⁰	0.16	
	C1C2-PAA2k			14.6			370000	211.46	1.54.10 ⁻⁹	0.74	
	S1S2C3-PAA2k			9.1			290000	86.5	1.03.10 ⁻⁹	0.22	
	C1C2C3C4S5-PAA5k			17.8			327000	292.6	2.74.10 ⁻⁹	0.97	
	S1-PAA2k			9			300000	69.8	7.8.10 ⁻¹⁰	0.23	
	C1C2C3		adsorbed H ⁺ only	15.1			342000	181.6	1.55.10 ⁻⁹	0.73	
	C1S2S3			14.8			333000	166	1.50.10 ⁻⁹	0.68	
	C1S2			13.2			328000	205	1.90.10 ⁻⁹	0.53	
	C1C2C3C4-cit			Citrate			15.9	312000	133.3	1.37.10 ⁻⁹	0.73
Jung et al [13]	AMI227 Ferumoxtran Sinerem (brand names)	γ -Fe ₂ O ₃ /Fe ₃ O ₄ mixture	Hydrophilic Polymer (Dextran)	6.2	TEM-d _w	1	339000	53	4.6.10 ⁻¹⁰	0.13	
Koenig et al [9]	MION46L Clariscan (brand names)			8.05	VSM	1	274000	44	5.9.10 ⁻¹⁰	0.17	
Forge et al [8]	250 Gauss	γ -Fe ₂ O ₃	aminopropyl-trimethoxy-silane	10.4	VSM	1	326000	133	1.24.10 ⁻⁹	0.33	
	1000 Gauss			9.6			332000	95.2	8.64.10 ⁻¹⁰	0.29	
	2000 Gauss			8.4			306000	54.7	5.84.10 ⁻¹⁰	0.20	
Lartigue et al [10]	Rha-4	γ -Fe ₂ O ₃	rhamnose-phosphonate	4.6	NMRD	1	399000	42	2.64.10 ⁻¹⁰	0.08	
	Rha-10			10.3			363000	266	2.02.10 ⁻⁹	0.36	
	Rha-18			18.5			337000	292	2.57.10 ⁻⁹	1.1	
Tromsdorf et al [24]	4nm-PEG1100	Fe ₃ O ₄	PEG-phosphate	4	TEM	1	363000	17.5	1.3.10 ⁻¹⁰	0.05	
	6nm-PEG1100			6			42	3.2.10 ⁻¹⁰	0.12		
Martina et al [19]	Conventional MFL	γ -Fe ₂ O ₃	Citrate-coated Magnetic Fluid encapsulated in Liposomes	300	DLS		5.10 ⁻⁴ [a]	177	67	1.08.10 ⁻⁶	0.15
	PEG-ylated MFL			202			2.6.10 ⁻³ [a]	896	124	4.06.10 ⁻⁷	0.34
				195			3.3.10 ⁻³ [a]	1150	130	3.24.10 ⁻⁷	0.41
Sanson et al [21]	WDi-20	γ -Fe ₂ O ₃	Hydrophobic Membrane of Polymersome (PTMC-PGA)	100	DLS		2.3.10 ⁻² [b]	6460	81	4.49.10 ⁻⁸	0.60
	WDi-35			90			4.4.10 ⁻² [b]	12200	134	3.93.10 ⁻⁸	0.92
Cheong et al [22]	oxide	γ -Fe ₂ O ₃	Dimercapto-succinic acid (DMSA)	15	TEM	1	350000	145	1.2.10 ⁻⁹	0.74	
Beaune et al [20]	DDAB magnetic vesicles: REV	γ -Fe ₂ O ₃	Oleic acid (OA)	150	TEM	1.6.10 ⁻² [c]	4200	177	1.6.10 ⁻⁷	0.87	

[a] From the iron/lipid molar ratio converted into a weight ratio inside the membrane. Assuming a lipid density of 1 and a membrane thickness of 3.5 nm, we deduced the volume of iron oxide inside the whole volume of the vesicle.

[b] From the feed weight ratios inside the membrane (20%, 35%, 50 % and 70%). Assuming a polymer density of 1 and a membrane thickness of 10 nm (SANS), we deduced the volume of iron oxide inside the whole volume of the vesicle.

[c] Measured by magnetophoresis. REV stands for “reverse phase evaporation”, ME for “multiple emulsion”, DDAB for didodecyldimethyl ammonium bromide. The USPIOs have a $d_w=7.5$ nm, $M_v=2.6.10^5$ A/m and $r_2=105$ s⁻¹.m.M⁻¹.

Reference	Sample code	Magnetic materials	Nature of coating	Size (nm)	Method	ϕ_{intra}	M_v (A·m ⁻¹)	r_2 (s ⁻¹ ·mM ⁻¹)	$\phi_{\text{intra}} \cdot r_2 \cdot M_v^{-2}$ (s ⁻¹ ·mM ⁻¹ A ⁻² ·m ²)	$\Delta\omega\tau_D$
In motional averaging regime – $\Delta\omega\tau_D < 1$ (continued)										
Pinho et al. ^[11]	FF (core)	γ -Fe ₂ O ₃	Porous SiO ₂	12.5	VSM ^[d]	1	282000	228	$2.11 \cdot 10^{-9}$	0.41
	0A			14	TEM	0.71	201000	100	$1.29 \cdot 10^{-9}$	0.37
	1A			27		0.1	27900	64	$6.37 \cdot 10^{-9}$	0.19
	2A			40		$3 \cdot 10^{-2}$	8550	47	$1.44 \cdot 10^{-8}$	0.13
	3A			50		$1.5 \cdot 10^{-2}$	4400	38	$2.24 \cdot 10^{-8}$	0.10
	4A			66		$6.8 \cdot 10^{-3}$	1920	23	$3.12 \cdot 10^{-8}$	0.08
	5A			114		$1.3 \cdot 10^{-3}$	370	15	$1.05 \cdot 10^{-7}$	0.04
	6A			145		$6.1 \cdot 10^{-4}$	170	12	$1.95 \cdot 10^{-7}$	0.03
Wang et al. ^[17]	IOs (Resovist)	γ -Fe ₂ O ₃	Hydrophilic Polymer (Dextran)	60	DLS	$8.4 \cdot 10^{-2}$ ^[e]	19500	282.4	$3.5 \cdot 10^{-8}$	0.65
	IO-loaded PLGA-mPEG		Amphiphilic Copolymer Micelle (PLGA-PEG)	233		$4 \cdot 10^{-3}$ ^[e]	1160	532.7	$8.8 \cdot 10^{-7}$	0.59
Taboada et al. ^[12]	S1	γ -Fe ₂ O ₃	Porous SiO ₂ (aerogel)	160	DLS	$1.1 \cdot 10^{-2}$	3180	148	$1.6 \cdot 10^{-7}$	0.76
	S2			120		$1.5 \cdot 10^{-2}$	4590	164	$1.16 \cdot 10^{-7}$	0.62
Out of motional averaging regime – $\Delta\omega\tau_D > 1$										
Taboada et al. ^[12]	S3	γ -Fe ₂ O ₃	Porous SiO ₂ (aerogel)	313	DLS	$1.2 \cdot 10^{-2}$	3880	326	$2.6 \cdot 10^{-7}$	3.6
This study	Clusters S1S2C	γ -Fe ₂ O ₃ cluster	Double Hydrophilic Copolymer (PAM-PTEA)	127	DLS	$9 \cdot 10^{-2}$	26000	91	$1.22 \cdot 10^{-8}$	3.9
Beaune et al. ^[20]	DDAB magnetic vesicles: ME	γ -Fe ₂ O ₃	Oleic acid (OA)	300	TEM	$8 \cdot 10^{-3}$ ^[c]	2100	185	$3.36 \cdot 10^{-7}$	1.6
This study	S2C14	γ -Fe ₂ O ₃ cluster	Double Hydrophilic Copolymer (PAM-PTEA)	132	DLS	$8.3 \cdot 10^{-2}$	24200	91	$1.29 \cdot 10^{-8}$	3.9
	S2C12			260		0.15	44000	216	$1.7 \cdot 10^{-8}$	28
	C1C2C3C4-PAA5k	γ -Fe ₂ O ₃ demixed droplet	Hydrophilic Polymer (PAA)	114		0.286	89000	427	$1.54 \cdot 10^{-8}$	10.8
Berret et al. ^[14]	PTEA(5k)	γ -Fe ₂ O ₃ cluster	Double Hydrophilic Block Copolymer (PAM-PTEA)	70	DLS	0.22	57200	74	$4.98 \cdot 10^{-9}$	2.2
	PTEA(11k)			170		0.38	99000	162	$6.28 \cdot 10^{-9}$	25
Xie et al. ^[18]	Loosen SPION cluster (A)	Fe ₃ O ₄ cluster	Oleic acid (OA) / Oleylamine in Amphiphilic Copolymer Micelle (PEG-PLA)	58	DLS	0.12 ^[f]	42000	117	$8 \cdot 10^{-9}$	1.3
	Condense cluster B			73				0.20 ^[f]	70000	233
	Condense cluster C			95		363	$1.48 \cdot 10^{-8}$			5.9
	Condense cluster D			97		413	$1.69 \cdot 10^{-8}$			6
	Condense cluster E			144		458	$1.87 \cdot 10^{-8}$			14
	Condense cluster F			199		512	$2.09 \cdot 10^{-8}$	26		

[d] We are in debt to the authors of this reference to have provided us their ferrofluid to make this VSM measurement. Volume fractions were calculated from TEM images. Relaxivities at 25 °C were rescaled by a factor 0.686/0.895.

[e] Calculated from the iron weight ratio measured by inductively coupled plasma mass spectroscopy (ICP-MS). The volume fractions enable to get the volume magnetizations using given values of specific magnetizations ($72.9 \text{ emu}\cdot\text{g}^{-1}$ for IOs and $83.5 \text{ emu}\cdot\text{g}^{-1}$ for IO-loaded PLGA-mPEG).

[f] Measured by thermogravimetry analysis (TGA). The USPIOs have a $d_w=10.5 \text{ nm}$ (TEM, $N=1822$) and $M_v=3.3 \cdot 10^5 \text{ A}\cdot\text{m}^{-1}$.

Reference	Sample code	Magnetic materials	Nature of coating	Size (nm)	Method	ϕ_{intra}	M_v (A·m ⁻¹)	r_2 (s ⁻¹ ·mM ⁻¹)	$\phi_{\text{intra}} \cdot r_2 \cdot M_v^{-2}$ (s ⁻¹ ·mM ⁻¹ A ⁻² ·m ²)	$\Delta\omega\tau_D$
Out of motional averaging regime – $\Delta\omega\tau_D > 1$ (continued)										
Ai et al ^[16]	8 nm SPIO PCL5k-b-PEG5k	Fe ₃ O ₄ cluster	Amphiphilic Copolymer Micelle (PEG-PCL)	97	DLS	0.11	41900	318	1.94·10 ⁻⁸	3.7
	16 nm SPIO PCL5k-b-PEG5k			110		0.19	79200	471	1.42·10 ⁻⁸	9
Cheong et al ^[22]	core/shell	Fe- γ Fe ₂ O ₃ core-shell	Dimercapto-succinic acid (DMSA)	15.4	TEM	1	660000 ^[g]	324	8.3·10 ⁻¹⁰	1.5
Paquet et al ^[15]	Densely packed SPIONS	γ -Fe ₂ O ₃ /Fe ₃ O ₄ mixture cluster	Surfactant (SDS)	68	TEM	0.34	98600	270	9.3·10 ⁻⁹	6
	SPION Cluster core inside a hydrogel shell	γ -Fe ₂ O ₃ /Fe ₃ O ₄ mixture cluster	Polymer (PNIPAM) Hydrophilic at T<32°C, Hydrophobic at T>32°C	88		0.157	45500	394	3·10 ⁻⁸	3.3
				112		0.076	22100	420	6.6·10 ⁻⁸	2.6
				130		0.049	14100	436	1.1·10 ⁻⁷	2.2
				108		0.085	24600	467	6.5·10 ⁻⁸	2.7
				152		0.03	8800	484	1.9·10 ⁻⁷	1.9
				176		0.02	5700	505	3.1·10 ⁻⁷	1.6
Jung et al ^[13]	AMI-25 Feridex Ferumoxide Endorem (brand names)	γ -Fe ₂ O ₃ /Fe ₃ O ₄ mixture cluster	Hydrophilic Polymer (Dextran)	80	DLS	0.23 ^[h]	77000	107	4.1·10 ⁻⁹	4.4
Yang et al ^[23]	Fe ₃ O ₄ -MMPNs	Fe ₃ O ₄ cluster	Amphiphilic Copolymer Micelle (PLGA-PEG)	73	TEM	0.118 ^[i]	45000	333	1.92·10 ⁻⁸	2.2
	MnFe ₂ O ₄ -MMPNs	MnFe ₂ O ₄ cluster		70		0.125 ^[j]	51000	567	2.78·10 ⁻⁸	2.3
Sanson et al ^[21]	WDi-50	γ -Fe ₂ O ₃	Hydrophobic Membrane of Polymersome (PTMC-PGA)	94	DLS	5.8·10 ⁻² ^[b]	16200	173	3.81·10 ⁻⁸	1.34
	WDi-70			104		7.1·10 ⁻² ^[b]	19800	182	3.27·10 ⁻⁸	2.0

[g] Core diameter is 9 nm, representing 18% of the particle volume. Alpha-iron density being 7.874 g·cm⁻³, an average mass density of the core-shell of 5.5 g·cm⁻³ was used to derive M_v from the mass magnetization of 115 emu·g⁻¹.

[h] 63.8 wt% iron oxide from thermogravimetry analysis (TGA). The USPIOs have a $d_w=5.6$ nm (TEM, $N=694$).

[i] 40.9 wt% iron ferrite from TGA. The USPIOs have $d_w=9$ nm (TEM), $M_v=3.3 \cdot 10^5$ A/m (74 emu·g⁻¹).

[j] 41.7 wt% manganese ferrite from TGA. The USPIOs have $d_w=9$ nm (TEM), $M_v=4.0 \cdot 10^5$ A/m (80.8 emu·g⁻¹).

Table 2. Saturation magnetizations, optimal diameters and maximum relaxivities for different types of magnetic particles used as T_2 MRI contrast agents.

Materials	M_v [$A \cdot m^{-1}$] ^[a]	d_{optimal} [nm] ^[b]	r_2^{max} [$s^{-1} \cdot mM^{-1}$] ^[c]
Maghemite nanoparticles	3.5×10^5	55	750
Clusters of maghemite nanoparticles at a volume dilution of 5 ($\phi_{\text{intra}}=20\%$ v/v maghemite fraction)	7×10^4	120	750
Iron-iron oxide core-shell nanoparticles	6.6×10^5	38	1200
$(Zn_{0.4}Mn_{0.6})Fe_2O_4$ nanoparticles	8.75×10^5	35	1860

[a] saturation magnetization

[b] optimal diameter

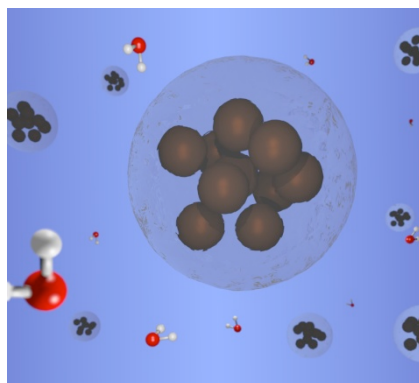
[c] maximum transverse relaxivity

Table of contents entry. This study evidences size, magnetization and magnetic volume fraction as the only control parameters of MRI T_2 contrast agents. Experimental relaxation and magnetometry data on magnetic particles draw up a master curve, allowing the prediction of the efficiency of any nanoparticles or clusters. A calculation of the optimal size for T_2 contrast agents of different natures is also performed.

Keyword list. Magnetic Resonance Imaging Contrast Agents; Transverse Relaxivity; Motional Averaging Regime; Static Dephasing Regime; Superparamagnetic Iron Oxide Nanoparticles

Quoc L. Vuong, Jean-François Berret, Jérôme Fresnais, Yves Gossuin* and Olivier Sandre*

Universal Scaling Law to Predict the Efficiency of Magnetic Nanoparticles as MRI T2-Contrast Agents



ToC figure

Supporting Information

for *Adv. Healthcare Mater.*, DOI: 10.1002/ adhm.201200078

Universal Scaling Law to Predict the Efficiency of Magnetic Nanoparticles as MRI T2-Contrast Agents

By

Quoc L. Vuong, Jean-François Berret, Jérôme Fresnais, Yves Gossuin and Olivier Sandre**

Dr. Q. L. Vuong, Author-One,
Université de Mons, Biological Physics Department, 20 Place du Parc, 7000 Mons, Belgium

Dr. J.-F. Berret, Author-Two,
Université Denis Diderot Paris-VII, CNRS UMR7057, Matière et Systèmes Complexes
10 rue Alice Domon et Léonie Duquet, 75013 Paris, France

Dr. J. Fresnais, Author-Three,
UPMC Univ Paris 06, CNRS UMR7195, Physicochimie, Colloïdes et Sciences Analytiques
4 place Jussieu, 75005 Paris, France

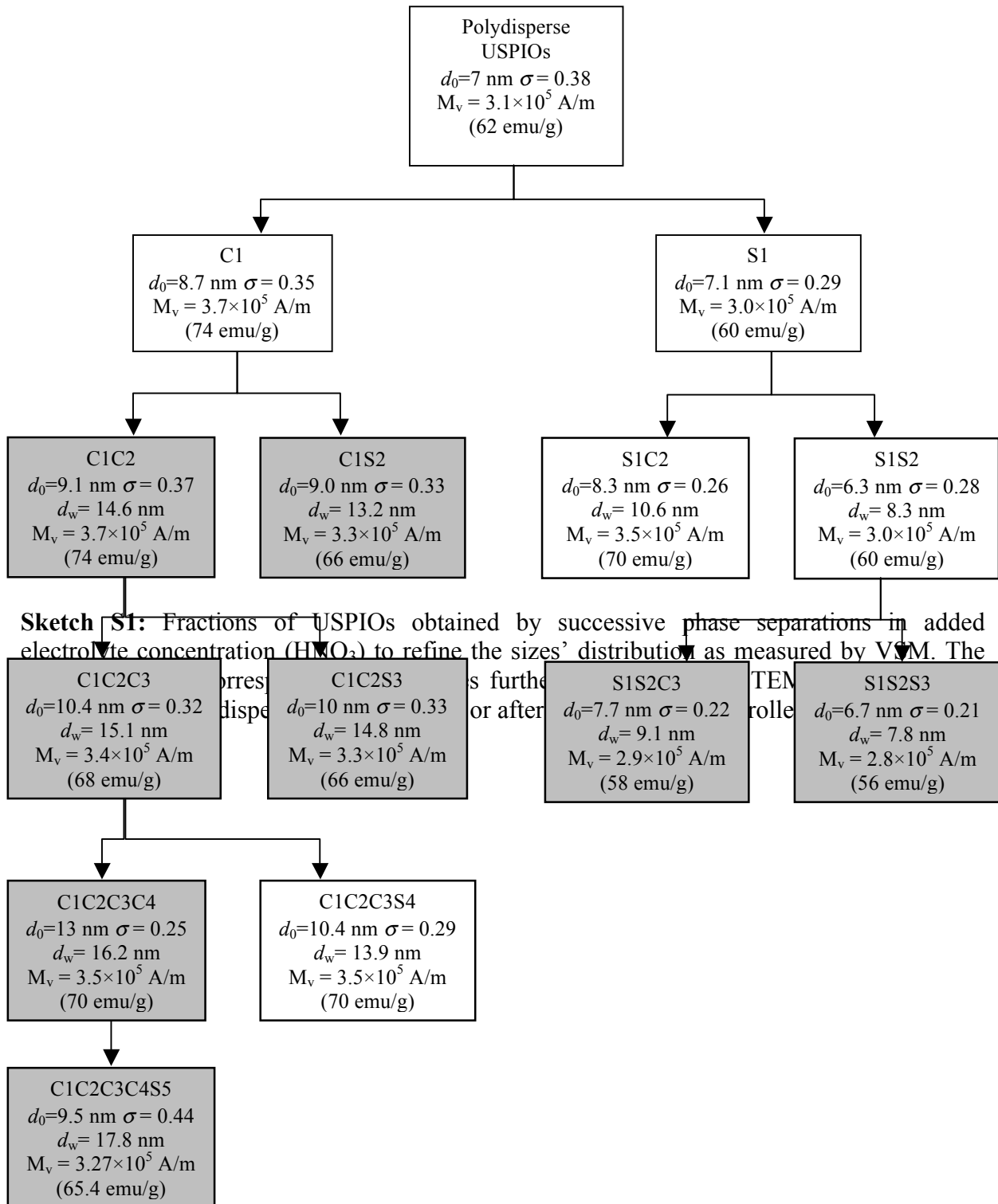
[*] Dr. Y. Gossuin, Corresponding-Author,
Université de Mons, Biological Physics Department, 20 Place du Parc, 7000 Mons, Belgium
E-mail: yves.gossuin@umons.ac.be

[*] Dr. O. Sandre, Corresponding-Author,
Université de Bordeaux, CNRS UMR5629, Laboratoire de Chimie des Polymères Organiques
ENSCBP, 16 Avenue Pey Berland, 33607 Pessac, France
E-mail: olivier.sandre@ipb.fr

Outline:

- S1. Synoptic scheme of the size sorting procedure
- S2. Characterization of the nanoparticles
 - a. Magnetometry
 - b. Transmission Electron Microscopy
 - c. NMR Relaxometry

S1. Synoptic scheme of the size sorting procedure

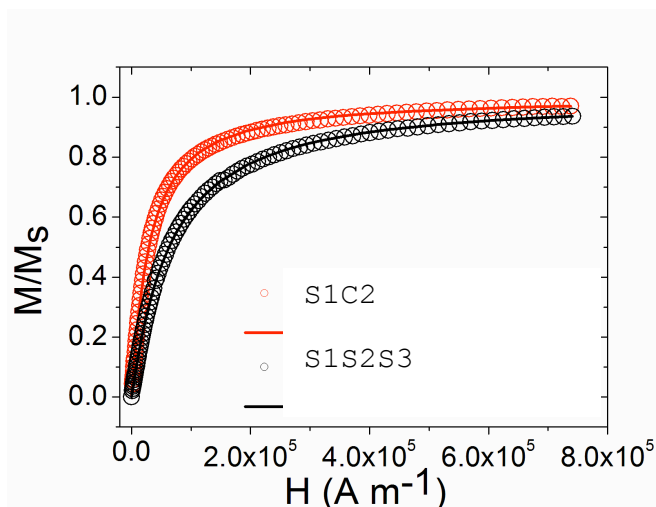


S2. Characterization of the nanoparticles

S2.a Magnetometry

We use two populations (S1S2S3 and S1C2) as a comparison. **Figure S1** shows the typical evolution of the macroscopic magnetization $M(H)$ normalized by its saturation value M_S for the γ -Fe₂O₃ superparamagnetic NP. Here, $M_S = f m_s$, where m_s is the specific magnetization of colloidal maghemite (approximately $m_s = 3.5 \times 10^5 \text{ A m}^{-1}$) which is lower than for bulk maghemite. It decreases when the diameter of the superparamagnetic NP decreases due to some disorder of the magnetic moments located near the surface. The solid curves on Figure S1 were obtained by Langevin fits convoluted with log-normal distribution laws of the particle sizes. The parameters of the distribution are the median diameter and the standard variations, respectively $d_0^{VSM} = 6.7 \pm 0.1 \text{ nm}$ with $\sigma^{VSM} = 0.21 \pm 0.03$ for S1S2S3 and $d_0^{VSM} = 8.3 \pm 0.1 \text{ nm}$ with $\sigma^{VSM} = 0.21 \pm 0.02$ for S1C2.

Figure S1: Magnetic field dependence of the macroscopic magnetization $M(H)$ normalized by its saturation value M_S for cationic maghemite dispersions. The solid curve was obtained using the Langevin function for superparamagnetism convoluted with a log-normal distribution function for the particle sizes, given with median diameters d_0^{VSM} and width σ^{VSM} .



S2.b Transmission Electron Microscopy (TEM)

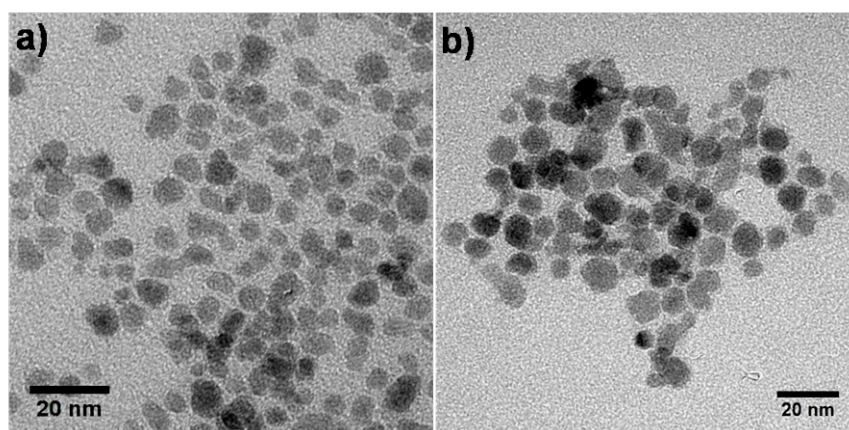


Figure S2: Iron oxide superparamagnetic NPs. (a) S1S2S3 and (b) S1C2 as observed by TEM. The stability of the dispersion was ensured by electrostatic interactions mediated by the native cationic charges in diluted HNO₃ (pH=1.2– 1.7).

In fact, the median diameter d_0^{VSM} obtained by VSM is related to the crystal structure inside the γ -Fe₂O₃ nanoparticle. We then compared these values with the physical diameters d_0^{TEM} by using image analysis of transmission electron microscopy (TEM). **Figure S2** displays images of the two batches of γ -Fe₂O₃ USPIOs chosen as examples (S1S2S3 and S1C2).

Figure S3 shows probability distribution functions of sizes for these NPs observed by TEM on a series of images similar to Figure S2. The data are fitted by a log-normal function with physical diameters $d_0^{TEM} = 6.8 \pm 0.2$ nm and $d_0^{TEM} = 9.3 \pm 0.2$ nm, with polydispersities $\sigma^{TEM} = 0.21 \pm 0.01$ and $\sigma^{TEM} = 0.18 \pm 0.01$.

$$p(d, d_0, \sigma_D) = \frac{1}{\sqrt{2\pi}\sigma_D d} \exp\left(-\frac{\ln^2(d/d_0)}{2(\sigma_D)^2}\right) \quad (S1)$$

These values are in good agreement with the ones obtained from VSM, albeit with a minor difference between the median diameter d_0^{VSM} and physical diameter d_0^{TEM} , which could originate from defects located close to the particles' surface not contributing to the magnetic properties.

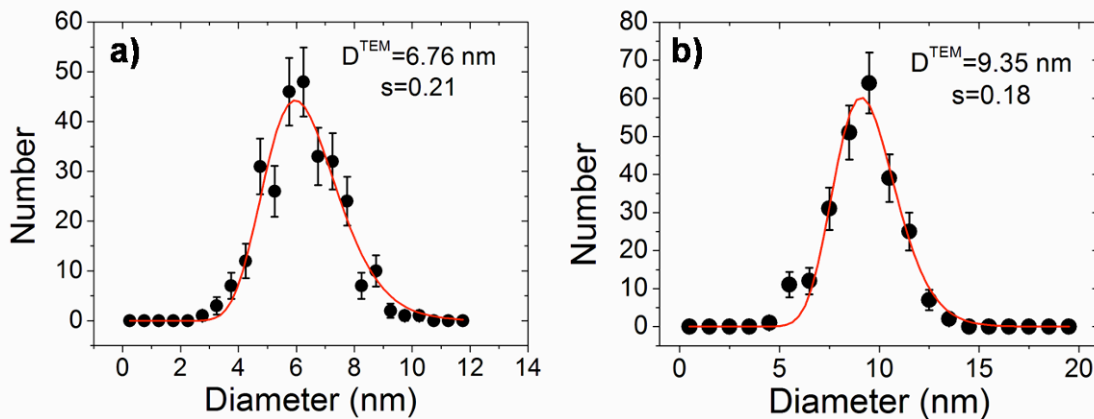
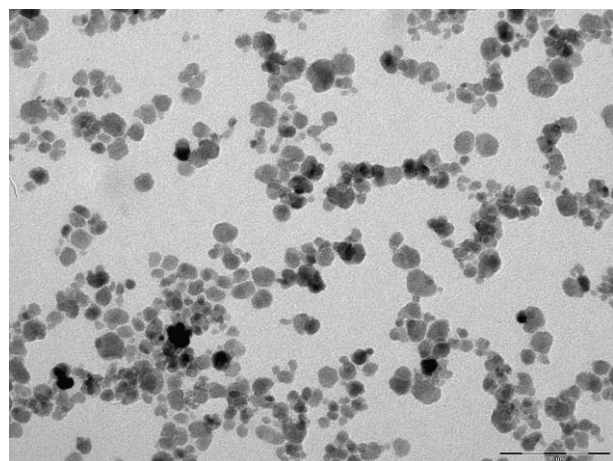
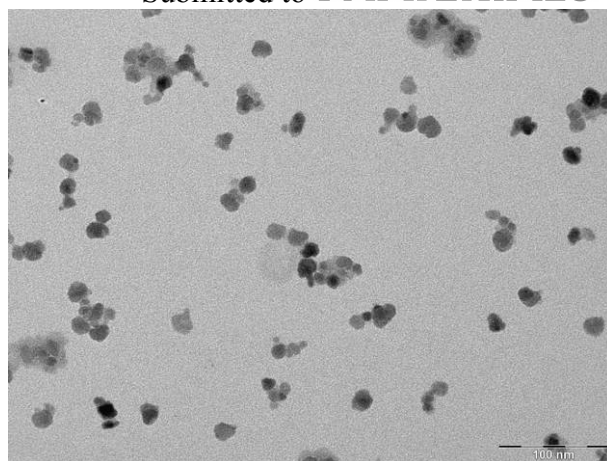


Figure S3: Probability distributions function of sizes for two γ -Fe₂O₃ USPIOs: a) S1S2S3; b) S1C2. The continuous line was derived from best fit calculation using a Log-normal distribution. For these dispersions, the average diameters by TEM were 6.8 nm and 9.3 nm, and the polydispersity 0.21 and 0.18.

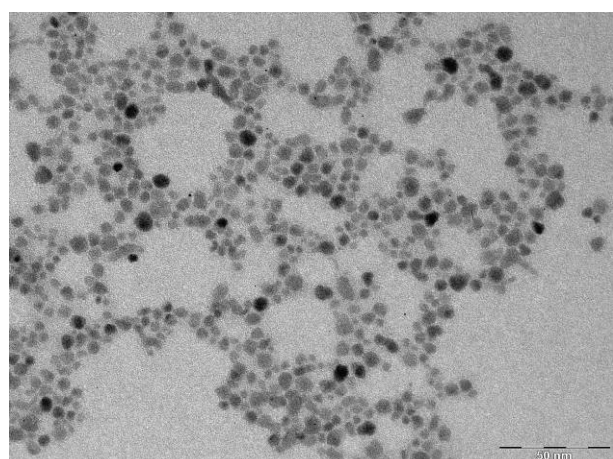
Using the Log-normal distributions deduced by VSM, we can estimate a weight-averaged diameter $d_w = \langle d^4 \rangle / \langle d^3 \rangle$ characteristic of each sample by calculating the 4th and 3th order moments of the Log-normal distributions: $d_w = d_0 \times \exp(3.5 \times \sigma^2)$. This fairly compares to the average diameter d_{TEM} obtained by the analysis of TEM pictures (Figure S3). From this comparison between TEM and VSM, we conclude that the weight average diameter d_w calculated from the two fitting parameters d_0 and σ of the VSM curve correctly reflects both the size distribution of the samples and their magnetic surface disorder and therefore can be used as a single characteristic size.



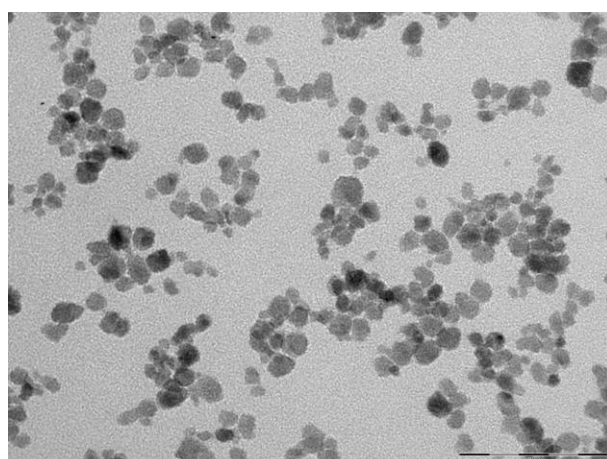
C1C2C3 in HNO₃ (pH 1.5)



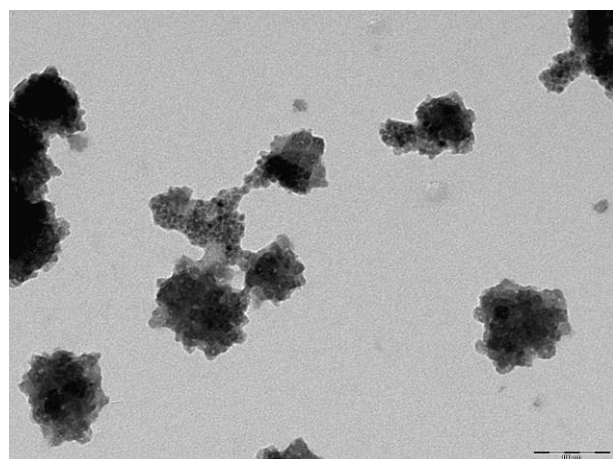
C1C2C3C4 in HNO₃ (pH 1.5)



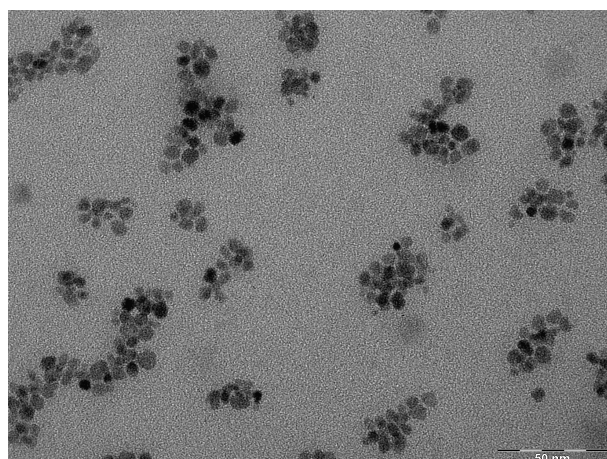
S1S2-citrate (pH 7)



C1C2S3 in HNO₃ (pH 1.5)



S1S2C3@PAA/PAM-*b*-PTEA clusters



S1S2S3@PAA/PAM-*b*-PTEA clusters

Figure S4: Typical TEM images of the synthesized particles. The images were acquired on a JEOL100 transmission electron microscope operating at 80 kV by Aude Michel, “Physicochimie des Electrolytes, Colloïdes et Sciences Analytiques” at UPMC Univ Paris 6.

S2.c NMR Relaxometry

Figure S5 shows the longitudinal NMRD profiles for all the (U)SPIO samples prepared in this study. As expected, the r_1 relaxivities at high fields are really low.

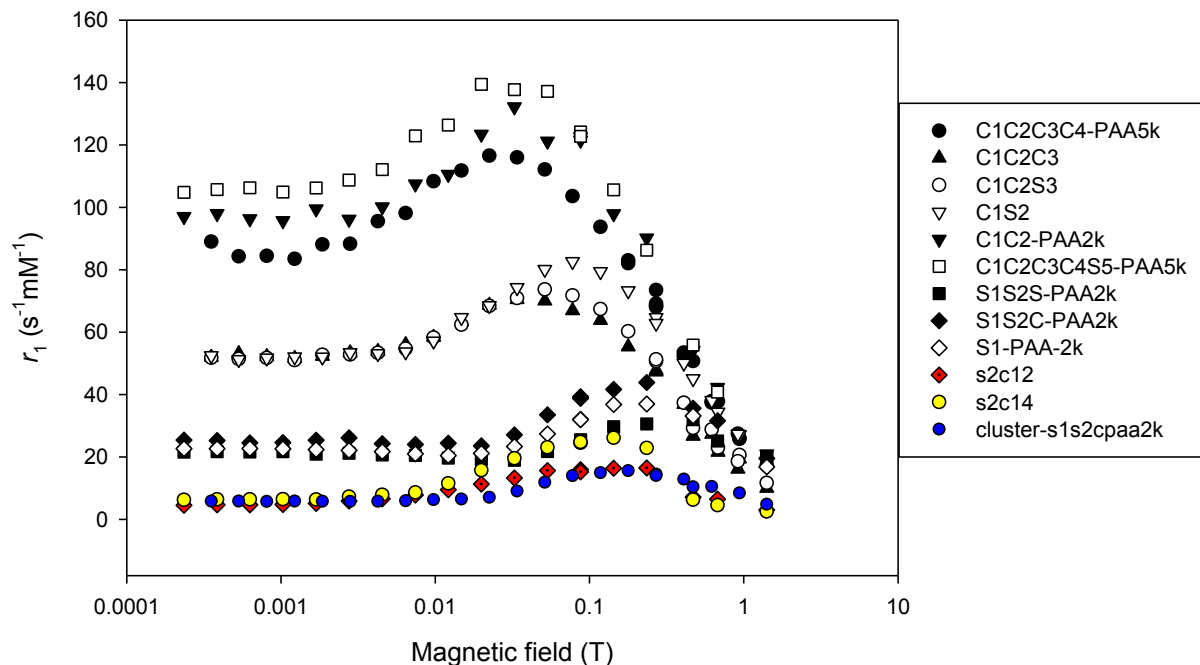


Figure S5: longitudinal relaxation of the samples at different magnetic fields.

The transverse relaxivity of all samples at different magnetic fields are shown on **Figure S6**. The relaxivity at 1.41 T was used in the article since it is close to classical clinical imaging fields. We also checked on some samples that the transverse relaxation was almost the same at 1.41 T and at very high fields (*e.g.* 9.4 T/400 MHz), as expected for maghemite particles.

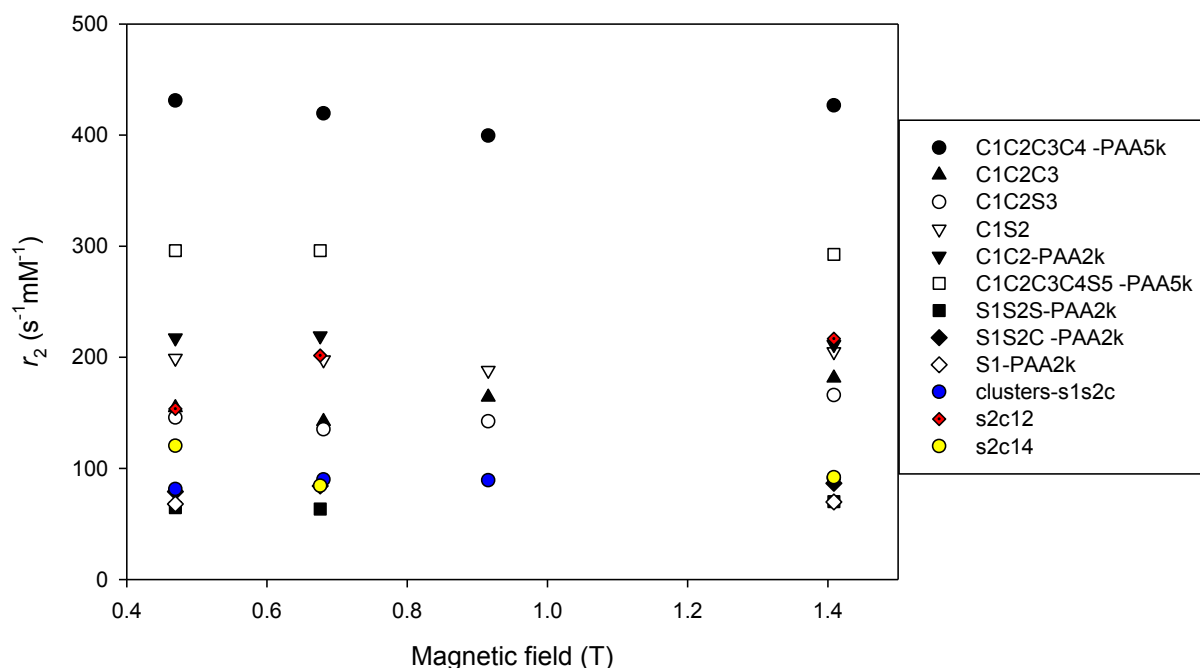


Figure S6: transverse relaxation of the samples at different magnetic fields.

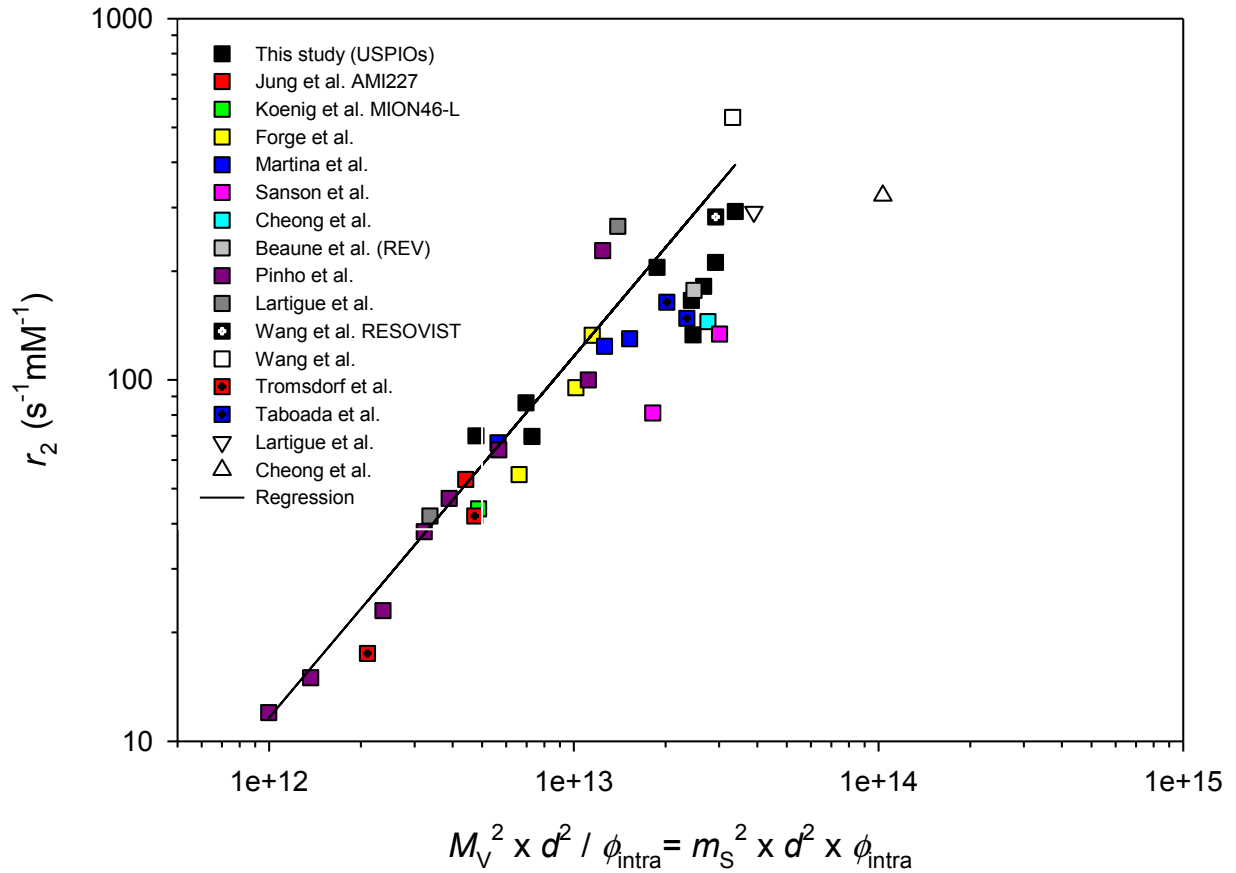


Figure S7: Raw values of the transverse relaxivity at high field ($\geq 1\text{T}$) for samples in the MAR. r_2 is appearing linear with the squares of the magnetization and of the diameter divided by the intra-aggregate volume fraction for individual USPIOs (for which $\phi_{\text{intra}}=100\%$) and clusters (either of low size or dilute) in the MAR *i.e.* satisfying Equation (4).

We can also introduce the specific magnetization of the magnetic cores in the cluster m_S and relate it to the whole body magnetization $M_v = \phi_{\text{intra}} \times m_S$. Then the transverse relaxivity r_2 becomes linear with $m_S^2 \times d^2 \times \phi_{\text{intra}}$ in the MAR. The other clusters corresponding to $\Delta\omega\tau_D > 1$ exhibit a lower r_2 than the power law and saturate below a plateau value given by Table 2.